SPRINGER BRIEFS IN
APPLIED SCIENCES AND TECHNOLOGY

Eva Barreira
Ricardo M. S. F. Almeida

Infrared Thermography for Building Moisture Inspection

Springer

SpringerBriefs in Applied Sciences and Technology

SpringerBriefs present concise summaries of cutting-edge research and practical applications across a wide spectrum of fields. Featuring compact volumes of 50–125 pages, the series covers a range of content from professional to academic.

Typical publications can be:

- A timely report of state-of-the art methods
- An introduction to or a manual for the application of mathematical or computer techniques
- A bridge between new research results, as published in journal articles
- A snapshot of a hot or emerging topic
- An in-depth case study
- A presentation of core concepts that students must understand in order to make independent contributions

SpringerBriefs are characterized by fast, global electronic dissemination, standard publishing contracts, standardized manuscript preparation and formatting guidelines, and expedited production schedules.

On the one hand, **SpringerBriefs in Applied Sciences and Technology** are devoted to the publication of fundamentals and applications within the different classical engineering disciplines as well as in interdisciplinary fields that recently emerged between these areas. On the other hand, as the boundary separating fundamental research and applied technology is more and more dissolving, this series is particularly open to trans-disciplinary topics between fundamental science and engineering.

Indexed by EI-Compendex, SCOPUS and Springerlink.

More information about this series at http://www.springer.com/series/8884

Eva Barreira · Ricardo M. S. F. Almeida

Infrared Thermography for Building Moisture Inspection

Springer

Eva Barreira
CONSTRUCT-LFC, Department of Civil Engineering, Faculty of Engineering
University of Porto
Porto, Portugal

Ricardo M. S. F. Almeida
CONSTRUCT-LFC, Department of Civil Engineering, Faculty of Engineering
University of Porto
Porto, Portugal

and

Department of Civil Engineering, School of Technology and Management
Polytechnic Institute of Viseu
Viseu, Portugal

ISSN 2191-530X ISSN 2191-5318 (electronic)
SpringerBriefs in Applied Sciences and Technology
ISBN 978-3-319-75385-0 ISBN 978-3-319-75386-7 (eBook)
https://doi.org/10.1007/978-3-319-75386-7

Library of Congress Control Number: 2018957663

This Springer imprint is published by the registered company Springer Nature Switzerland AG
The registered company address is: Gewerbestrasse 11, 6330 Cham, Switzerland

Preface

Moisture is one of the most deteriorating factors of buildings. Tracing it, using non-destructive techniques, is an obvious advantage, especially for buildings in use. The problem of moisture in buildings has always aroused great interest. Moisture damage may occur both due to the presence of moisture itself and/or due to its evaporation. Besides the degradation of materials and components, compromising their performance, durability, mechanical resistance, waterproofness and appearance, it can also cause poor indoor conditions resulting from biological growth.

Moisture content is traditionally assessed using destructive procedures, which require collecting a wall sample to be weighed in the laboratory. However, moisture content can also be assessed using non-destructive techniques as moisture detectors. These techniques may not be as accurate as the destructive procedures; however, they are very easy to use and deliver real-time results. Infrared thermography (IRT) is a non-contact and non-destructive testing technology that can be applied to determine the surface temperature of an object. Nevertheless, the procedures to detect moisture in building components using IRT are still under development as it is not clear if it can be used to detect moisture before any visible marks occur. However, changes in moisture content are related to changes in surface temperature and can, therefore, be detected by IRT, due to three physical phenomena: evaporative cooling at the moist area; reduced thermal resistance; and increased heat storage capacity of the moist material.

The main benefit of this book is that it provides a discussion about the opportunities and limitations of IRT to assess moisture-related pathologies in buildings using several practical models as example cases. Its special features are: (a) a state of the art of buildings-related IRT applications with the main focus on moisture assessment; and (b) practical discussion of several case studies, namely (b1) several set-ups and boundary conditions were created to compare IRT with other surface temperature measurement techniques and to understand the ideal conditions for accurate IRT; (b2) IRT was used to assess capillary absorption on a full-scale laboratory model and the drying process; (b3) IRT was used to assess moisture in walls due to wind-driven rain infiltrations in buildings in use; and (b4) IRT was used to assess the drying process of exterior walls.

This subject is appealing to the scientists, the engineers and the students. At the same time, this book will be going to the encounter of a variety of scientific and engineering disciplines, such as civil engineering, architecture, physics.

This work was financially supported by Project POCI-01-0145-FEDER-007457—CONSTRUCT—Institute of R&D In Structures and Construction funded by FEDER funds through COMPETE2020—Programa Operacional Competitividade e Internacionalização (POCI)—and by national funds through FCT—Fundação para a Ciência e a Tecnologia. The authors would also like to acknowledge their gratitude for the support received from the University of Porto—Faculty of Engineering, Portugal. Finally, the authors would welcome comments, corrections and suggestions of the readers with the aim of improving any future editions.

Viseu, Portugal Eva Barreira
Porto, Portugal Ricardo M. S. F. Almeida

Contents

Symbols and Units

c	Specific heat capacity (J kg^{-1} K^{-1})
h	Height (cm)
t	Time (h)
RH	Relative humidity (%)
Solar Rad	Solar radiation (W m^{-2})
T	Temperature (°C)
Wind Vel	Wind velocity (m s^{-1})
Wind Dir	Wind direction (º)

Greek Letters

ε	Emissivity (–)
λ	Thermal conductivity (W m^{-1} K^{-1})
ρ	Density (kg m^{-3})

Chapter 1
Introduction

1.1 Motivation

Moisture is one of the main causes of pathologies in buildings and, thus, has always aroused great interest within the scientific community. The damage in buildings can occur both due to the presence of moisture itself or due to its evaporation. In fact, moisture and the drying process may cause the degradation of building materials and components, compromising their performance concerning durability, mechanical resistance, waterproofness and appearance. Moisture can also cause unhealthy conditions for users, either due to the biological growth or due to the degradation of building materials and components.

Moisture may have different causes, which can be grouped as follows: built-in moisture; rising damp; infiltrations due to wind-driven rain; surface condensations; moisture due to hygroscopic phenomena and moisture due to accidental causes.

An early diagnosis is crucial to avoid severe degradation. Indeed, it is imperative to detect moisture in an earlier stage, i.e. before significant visible signs occur, and to trace the leak through the building elements. The use of non-destructive techniques to detect moisture can be very useful, especially when the building is occupied, as further work and greater costs are avoided during the assessment.

Infrared thermography (IRT) is a non-contact and non-destructive testing technology that allows the evaluation of thermal behaviour of existing buildings and identification of potential problems (Maldague 1994; Hart 2001; Bagavathiappan et al. 2013). It converts the infrared radiation emitted from bodies into thermal images, showing the temperature distribution of the surface (Maldague 2001; Rao 2008), as shown in Fig. 1.1. Nowadays, from a practical point of view, this technique is mainly used considering only a qualitative evaluation of the results, based on the simple observation of the thermal images. However, the scientific community has been working in new quantitative approaches, which are more often related to the evaluation of the temperature differences between areas with and without thermal anomaly (Maldague 2002; Lai and Poon 2012; Vavilov 2014).

E. Barreira and R. M. S. F Almeida, *Infrared Thermography for Building Moisture Inspection*, SpringerBriefs in Applied Sciences and Technology,
https://doi.org/10.1007/978-3-319-75386-7_1

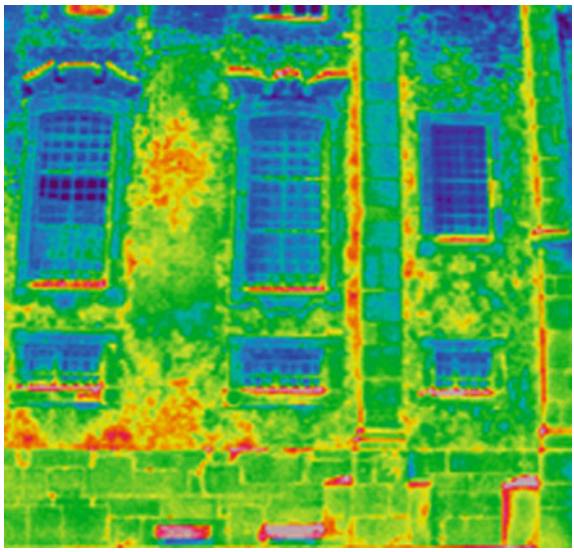

Fig. 1.1 Thermograph of a façade located in Porto, Portugal

However, IRT has several potential applications that have not yet been completely explored, such as detecting moisture in building components. Some authors have been working in this topic, proving that it is possible to use it to identify moisture in building elements as, for example, Balaras and Argiriou (2002), Avdelidis et al. (2003). However, only very few were able to establish a criterion for a quantitative assessment of the problem. Even when an attempt was made, the criteria and procedures were applied to a specific case study and its generalization to other building elements is not straightforward.

Therefore, it is still required additional research concerning the applicability of IRT to detect moisture and to characterize its consequences in building components. In this book, information relevant to this topic is collected and systematized, namely new work developed by the scientific community regarding detection of moisture in building materials and components using IRT is gathered, and it discusses the opportunities and limitations of IRT to assess moisture-related buildings pathologies using several practical models as example cases.

1.2 Main Developments on Using IRT to Assess Moisture

Two approaches can be applied to obtain the distribution of the surface temperature using infrared (IR) cameras: the passive and the active approach (Maldague 1993). Thermal images can be analysed qualitatively or quantitatively (Hart 2001). The quality of the thermal images can be affected by several parameters related to materials properties and to ambient conditions: (a) emissivity, which is crucial if

a quantitative analysis is required (Avdelidis and Moropoulou 2003); (b) surface colour as it can mask defects (Barreira and Freitas 2007); (c) reflections on metal and glazed surfaces (surfaces with high reflectance) (Barreira and Freitas 2007); (d) meteorological conditions such as air temperature, precipitation, wind speed, cloud cover and direct sunlight (Chew 1998); (e) heat sources near the measurement area (Hart 2001); (f) period of the day (day or night) and time of year (summer or winter conditions) (Chew 1998); (g) distance between camera and target, which may attenuate thermal radiation and affects the images clarity and precision, for distances above 10 m (Chew 1998).

This technology has been applied to buildings for a couple of decades to evaluate their performance (Hart 2001). IRT has been used to assess the floor covering comfort (Barreira and Freitas 2007), to detect insulation defects (Hart 2001), air leaks (Taylor et al. 2013; Barreira et al. 2017a; Lerma et al. 2018) and thermal bridges (Asdrubali et al. 2012), to evaluate thermal performance (Katunsky et al. 2013) and to inspect construction details (Cerdeira et al. 2011). IRT has also been used as a conservation evaluation tool for historic buildings treatments (Avdelidis and Moropoulou 2004), to detect defects in façades (Edis et al. 2014; Freitas et al. 2014) and as an inspection technique for frescoes assessment (Paoletti et al. 2013; Sfarra et al. 2016). The use of IRT in inspection procedures is well defined in standards such as ISO 6781 (1983), EN 13187 (1998) and ASTM-C 1060-90 (2003). A detailed comparison between the performances of different IR cameras can also be found in the literature (Bauer et al. 2015).

Some attempts of applying IRT to detect moisture in building components were already published, although mostly using only the qualitative approach (Balaras and Argiriou 2002; Avdelidis et al. 2003; Edis et al. 2014; Menezes et al. 2015). Nevertheless, the procedures to detect moisture in building components using IRT are still under discussion since it is still not clear if this technique can be used to detect moisture before any visible marks occur, such as efflorescence, biological growth, detachments or degradation of the material, and to trace a water leak through the building element. In addition, the potential of quantitative approaches applied to detect moisture in building materials and components remains largely untapped.

Changes in moisture content are related to changes in surface temperature and therefore can be detected by IRT, due to three physical phenomena:

- Evaporative cooling at the moist area: The evaporation at the surface is an endothermic reaction, which induces a decrease on the surface temperature (Rosina and Ludwig 1999; Avdelidis et al. 2003; Barreira and Freitas 2007; Grinzato et al. 2010; Bison et al. 2011a, b; Grinzato et al. 2011; Camino et al. 2014; Lerma et al. 2014; Barreira et al. 2016, 2017b).
- Reduced thermal resistance: The heat flow through wet materials is higher than through dry materials, which creates a heterogeneous thermal pattern as the surface temperature over the wet material is higher, if the inspection is made from the outside during the colder season. This effect is pushed to extremes when the wetting occurs in thermal insulation materials (Rajewski and Devine 1996; Edis et al. 2014, 2015).

- Increased heat storage capacity of the moist material: The surface temperature over a wet area responds more slowly to a change in the air temperature than the surface temperature over a dry area. Thus, when the whole surface is cooling, wet areas will cool more slowly. During the course of a sunlit day, wet areas will store more solar energy than dry areas; thus, they will cool more slowly during the evening (Balaras and Argiriou 2002; Lerma et al. 2011; Edis et al. 2014, 2015).

From the above references, only a few were able to establish a criterion for a quantitative assessment of the problem. In those studies, the moisture content was assessed using different physical principles (evaporative cooling of the surface and increased heat storage capacity).

The quantitative analysis of the results of IRT can be carried out using the following techniques: principal component thermography (PCT), pulsed phase thermography (PPT), differential absolute contrast (DAC), thermographic signal reconstruction (TSR), full width at half maximum (FWHM) and higher order statistics thermography (HOST). Although having great potential, as they tend to minimize the influence of emissivity variation, environmental reflections, etc., they are still not widespread and may not always be applicable, especially during long-term monitoring where large areas are covered. In addition, the equipment that generally is required is also more complex and expensive.

From the literature review, one can state that assessing moisture-related phenomena by IRT is possible, yet difficult, especially if a quantitative evaluation is intended. In this area, the methodologies and the potential of IRT for qualitative approaches are stabilized but, on the other hand, a well-defined methodology for a quantitative approach is still an open issue that requires attention from the scientific community.

This book presents the results of several experimental campaigns where the potential of IRT for moisture assessment is evaluated. An analysis for tackling the parameters that can affect IRT accuracy was carried out, and the applicability of IRT to assess moisture and drying in building components was analysed both in indoor and outdoor conditions.

References

Asdrubali F, Baldinelli G, Bianchi F (2012) A quantitative methodology to evaluate thermal bridges in buildings. Appl Energy 97:365–373

ASTM-C 1060–90 (2003) Standard practice for thermographic inspection of insulation installations in envelope cavities of frame buildings. ASTM International, USA

Avdelidis N, Moropoulou A (2003) Emissivity considerations in building thermography. Energy Buildings 35(7):663–667

Avdelidis N, Moropoulou A (2004) Applications of infrared thermography for the investigation of historic structures. J Cult Heritage 5(1):119–127

Avdelidis N, Moropoulou A, Theoulakis P (2003) Detection of water deposits and movement in porous materials by infrared imaging. Infrared Phys Technol 44(3):183–190

Bagavathiappan S, Lahiri B, Saravanan T, Jayakumar J (2013) Infrared thermography for condition monitoring—A review. Infrared Phys Technol 60:35–55

Balaras C, Argiriou A (2002) Infrared thermography for building diagnostics. Energy Buildings 34(2):171–183

Barreira E, Almeida RMSF, Delgado JMPQ (2016) Infrared thermography for assessing moisture related phenomena in building components. Constr Building Mater 110:251–269

Barreira E, Almeida RMSF, Ferreira JPB (2017a) Assessing the humidification process of lightweight concrete specimens through infrared thermography. Energy Procedia 132:213–218

Barreira E, Almeida RMSF, Moreira M (2017b) An infrared thermography passive approach to assess the effect of leakage points in buildings. Energy Buildings 140:224–235

Barreira E, Freitas VP (2007) Evaluation of building materials using infrared thermograph. Constr Building Mater 21(1):218–224

Bauer E, Freitas VP, Mustelier N, Barreira E, Freitas SS (2015) Infrared thermography—evaluation of the results reproducibility. Structural Survey 33(1):20–35

Bison P, Cadelano G, Capineri L, Capitani D, Casellato U, Faroldi P, Grinzato E, Ludwig N, Olmi R, Priori S, Proietti N, Rosina E, Ruggeri R, Sansonetti A, Soroldoni L, Valentini M (2011a) Limits and advantages of different techniques for testing moisture content in masonry. Mater Eval 69(1):111–116

Bison P, Cadelano G, Grinzato E (2011b) Thermographic signal reconstruction with periodic temperature variation applied to moisture classification. Quant Infrared Thermography J 8(2):221–238

Camino MS, León FJ, Llorente A, Olivar JM (2014) Evaluation of the behaviour of brick tile masonry and mortar due to capillary rise of moisture. Mater de Construcción 64(314):020

Cerdeira F, Vázquez ME, Collazo J, Granada E (2011) Applicability of infrared thermography to the study of the behaviour of stone panel as building envelopes. Energy Buildings 43:1845–1851

Chew M (1998) Assessing building façades using infra-red thermography. Structural Survey 16(2):81–86

Edis E, Flores-Colen I, Brito J (2014) Passive thermographic detection of moisture problems in façades with adhered ceramic cladding. Constr Building Mater 51:187–197

Edis E, Flores-Colen I, Brito J (2015) Quasi-quantitative infrared thermographic detection of moisture variation in facades with adhered ceramic cladding using principal component analysis. Building Environ 94:97–108

EN 13187 (1998) Thermal performance of buildings—Qualitative detection of thermal irregularities in building envelops—Infrared method. European Committee for Standardization, Belgium

Freitas SS, Freitas VP, Barreira E (2014) Detection of façade plaster detachments using infrared thermography—A non-destructive technique. Construction Building Mater 70:80–87

Grinzato E, Cadelano G, Bison P (2010) Moisture map by IR thermography. J Modern Optics 57(18):1770–1778

Grinzato E, Ludwig N, Cadelano G, Bertucci M, Gargano M, Bison P (2011) Infrared thermography for moisture detection: a laboratory study and in-situ test. Mater Eval 69(1):97–104

Hart J (2001) A practical guide for infra-red thermography for building surveys. BRE, UK

ISO 6781 (1983) Thermal Insulation—Qualitative detection of thermal irregularities in building envelopes—Infrared method. International Organization for Standardization, Switzerland

Katunsky D, Korjenic A, Katunska J, Lopusniak M, Korjenic S, Doroudiani S (2013) Analysis of thermal energy demand and saving in industrial buildings: a case study in Slovakia. Building Environ 67:138–146

Lai WL, Poon CS (2012) Boundary and size estimation of debonds in external wall finishes of high-rise buildings using Infrared thermography, In: Proceedings of QIRT2012—11th international conference on quantitative infrared thermography, Naples, Italy, June 2012

Lerma C, Barreira E, Almeida RMSF (2018) A discussion concerning active infrared thermography in the evaluation of buildings air infiltration. Energy Buildings 168:56–66

Lerma J, Cabrelles M, Portalés C (2011) Multitemporal thermal analysis to detect moisture on a building façade. Construction Building Mater 25(5):2190–2197

Lerma C, Mas Á, Gil E, Vercher J, Peñalver MJ (2014) Pathology of building materials in historic buildings. Relationship between laboratory testing and infrared thermography. Materiales de Construcción 64(313):009

Maldague X (1993) Nondestructive evaluation of materials by infrared thermography. Springer-Verlag, Germany
Maldague X (1994) Nondestructive testing monographs and tracts. Infrared methodology and technology. Gordon and Breach Science Publishers, Switzerland
Maldague X (2001) Theory and practice of infrared technology for nondestructive testing. Wiley-Interscience Publication, USA
Maldague X (2002) Applications of infrared thermography in nondestructive evaluation, Research Working Paper No. G1K7P4, University of Laval, Electrical and Computing Engineering Department, Canada
Menezes A, Gomes MG, Flores-Colen I (2015) In-situ assessment of physical performance and degradation analysis of rendering walls. Constr Building Mater 75:283–292
Paoletti D, Ambrosini D, Sfarra S, Bisegna F (2013) Preventive thermographic diagnosis of historical buildings for consolidation. J Cultural Heritage 14:116–121
Rajewski G, Devine G (1996) Building envelope—Infrared thermography—Preventative roof maintenance. Building Operator Association, Canada
Rao P (2008) Infrared thermography and its applications to civil engineering. Indian Concrete J 82(5):41–50
Rosina E, Ludwig N (1999) Optimal thermographic procedures for moisture analysis in building materials. Soc Photographic Instrumentation Eng (SPIE) 3827:22–33
Sfarra S, Ibarra-Castanedo C, Tortorac M, Arrizzac L, Cerichellic G, Nardia I, Maldague X (2016) Diagnostics of wall paintings: A smart and reliable approach. J Cultural Heritage 18:229–241
Taylor T, Counsell J, Gill S (2013) Energy efficiency is more than skin deep: Improving construction quality control in new-build housing using thermography. Energy Buildings 66:222–231
Vavilov V (2014) Noise-limited thermal/infrared nondestructive testing. NDT E Int 61:16–23

Chapter 2
Measurement of Surface Temperature Using Different Devices

2.1 Aim

As reported by several authors (Chew 1998; Hart 2001; Avdelidis and Moropoulou 2003; Barreira and Freitas 2007), there are several parameters that can influence significantly the measurement of surface temperatures using IRT. For that reason, this issue is deeply discussed in this chapter, including a comparison between the values obtained using three different devices (infrared camera, infrared thermometer and type T thermocouples).

The chapter describes the methodology and the results attained in two experimental campaigns, one in situ (IS) and the other one in laboratory (L). In the in situ case studies, the surface temperature of various finishing materials on the façades of a building was measured in different periods of the day and at different distances. This campaign included four case studies. The second campaign (laboratory) consisted in selecting materials with different emissivity, and exposing them to external environmental conditions, while measuring their surface temperature.

2.2 Materials and Techniques

During the test campaigns, an infrared camera, an infrared thermometer and type T thermocouples connected to a data logger were used. Before the measurements were carried out, calibration procedures were performed according to the operation manual of each device.

The main technical specifications of the thermographic camera used during the experimental campaigns (Fig. 2.1a) are presented in Table 2.1. An adequate tripod (Fig. 2.1b) guaranteed the stabilization of the camera during the tests. Reflection calibration and ambient and background compensation were assessed before each

E. Barreira and R. M. S. F Almeida, *Infrared Thermography for Building Moisture Inspection*, SpringerBriefs in Applied Sciences and Technology,
https://doi.org/10.1007/978-3-319-75386-7_2

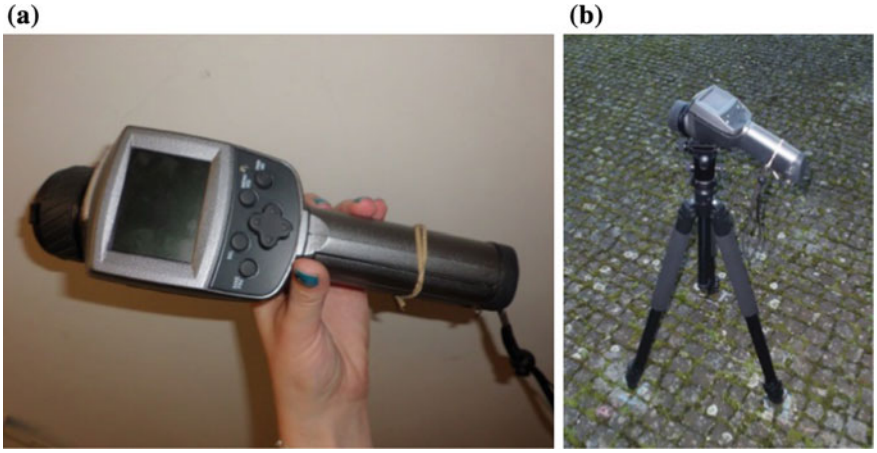

Fig. 2.1 **a** Infrared camera; **b** position of the camera during the measurements

Table 2.1 Specifications of the infrared camera

	Infrared camera
Measuring range	−20 to 250 °C
Resolution	0.1 °C
Accuracy	±2 °C or ±2% of reading
Detector	Uncooled focal plane array (microbolometer)
Spectral range	7.5–13 μm
Thermal image pixels	320 (H) × 240 (V) pixels
Focusing range	50 cm to infinite
IFOV	1.5 mrad

Table 2.2 Specifications of the infrared thermometer

	Infrared thermometer
Measuring range	−40–550 °C
Resolution	0.1 °C
Accuracy	±1 °C or ±1% of reading
Spectral range	8–4 μm
Distance to spot size (D:S)	12:1

measurement. The thermograms were treated using specific software, allowing the analysis, digital processing and archiving of the images captured by the camera.

The infrared thermometer is also a non-contact and non-destructive tool, which allows the measurement of the surface temperature of a single point on a material. The technical specifications of the device (Fig. 2.2a, b) can be found in Table 2.2.

A thermocouple is an electrical device that produces a temperature-dependent voltage as a result of the thermoelectric effect. The voltage can be converted into

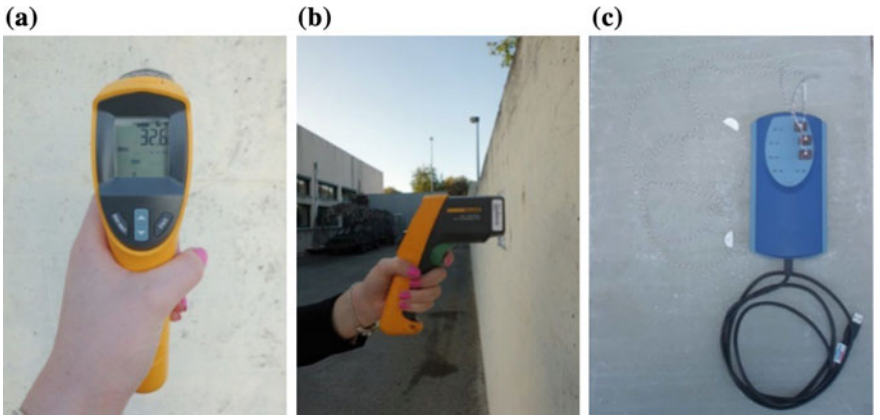

Fig. 2.2 **a** Infrared thermometer; **b** Position of the infrared thermometer during the measurements; **c** Data logger and type T thermocouples

temperature. Among the several models available on the market, the type T was selected for this work as it is a very stable thermocouple with a wide range of measurement (−200 to 350 °C).

The thermocouples were fixed to the surface of the materials with aluminium tape. In order to register and acquire the data from the thermocouples, a data logger was used (Fig. 2.2c). This device can be connected to a computer, and data is analysed using the data logger software. A 1 s interval was defined for the recording.

Two experimental campaigns, one in situ (IS) and the other in the laboratory (L), were implemented in order to compare the values measured by the different devices. The ambient conditions were varied throughout the tests as the measurements were made at different distances to the target (3, 9 and 15 m for IS and 3, 6 and 9 m for L) and in periods of the day with different luminosity, namely: (i)—direct solar radiation; (ii)—after sunset and (iii)—during night-time.

The first step of the procedure was defining the distances at which the thermograms were to be taken and marking the exact spot on the pavement. The thermocouples were then fixed to the surface and connected to the computer to begin data acquisition. Afterwards, the thermograms were taken at the desired distances, and finally, the infrared thermometer was used to measure the temperatures at different points.

It should be noted that with the infrared thermometer five temperature measurements were carried out and then the average value was calculated. Regarding the thermocouples, the data acquisition only ended when the measurement with the other two devices was completed, and at the end, the values were also averaged. The duration of the entire procedure was always less than 5 min.

In the in situ campaign, the surface temperature of three materials, with different emissivity, present on the façades of a building was measured. This campaign included four case studies (Fig. 2.3):

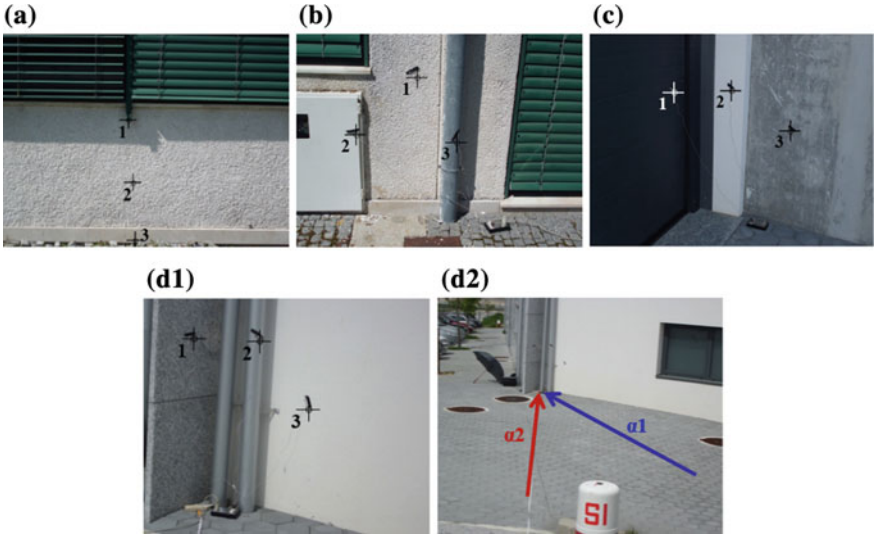

Fig. 2.3 Photograph of the case studies, including the location of the measuring points: **a** case study #01_IS; **b** case study #02_IS; **c** case study #03_IS; **d**1 case study #04_IS; **d**2 angles between the infrared camera and the target in case study #04_IS

- Case study #01_IS, where location "1" was on green lacquered aluminium, location "2" was on a projected coating mortar, and location "3" was on marble stone.
- Case study #02_IS, where location "1" was on a projected coating mortar, location "2" was on a metallic panel coated with white paint, and location "3" was on a galvanized steel downspout.
- Case study #03_IS, where location "1" was on a steel gate with rough surface, location "2" was on a white painted wall, and location "3" was on a concrete wall.
- Case study #04_IS was the last in situ example, and its geometry allowed including another parameter in the sensitivity analysis: the angle between the infrared camera and the target. The following three materials were evaluated in this case study: "1" for granite stone, "2" for a galvanized steel downspout and "3" for a white painted wall. Regarding the angle between the camera and the target, two values were tested, α1 and α2, as presented in Fig. 2.3d2.

Table 2.3 shows the input parameters used in the analysis of the thermal images, including the materials emissivity, the reflected temperature and the air temperature and relative humidity.

The laboratory campaign (L) consisted in selecting a group a commonly used construction materials, with different emissivity values, and exposing them to external environment conditions, while measuring their surface temperature. The specimens were placed against a wall ensuring that the incident solar radiation was identical and there were no reflections from nearby obstacles. The materials were grouped according to the following criteria:

Table 2.3 Emissivity, reflected temperature, air temperature and relative humidity for all in situ case studies

		ε	Reflected temperature (°C)			Air temperature (°C)			Relative humidity (%)		
			(i)	(ii)	(iii)	(i)	(ii)	(iii)	(i)	(ii)	(iii)
#01_IS	1	0.92	21.7	14.8	13.1	16.8	20.2	17.1	44.1	32.5	42.9
	2	0.87									
	3	0.93									
#02_IS	1	0.87	23.0	5.8	4.5	19.4	22.1	16.8	52.2	35.3	71.0
	2	0.92									
	3	0.28									
#03_IS	1	0.96	25.0	16.9	13.4	22.1	21.0	16.8	35.9	41.6	69.9
	2	0.92									
	3	0.93									
#04_IS	1	0.85	34.2* 32.9#	19.2* 14.5#	15.8* 12.8#	22.9* 22.7#	23.6* 23.6#	19.5* 19.4#	40.1* 39.8#	35.5* 35.4#	46.1* 45.9#
	2	0.28									
	3	0.92									

ε—Emissivity
(i)—Direct solar radiation; (ii)—after sunset; (iii)—during night-time
*—Case study #04_IS (Fig. 2.3d2): α1
#—Case study #04_IS (Fig. 2.3d2): α2

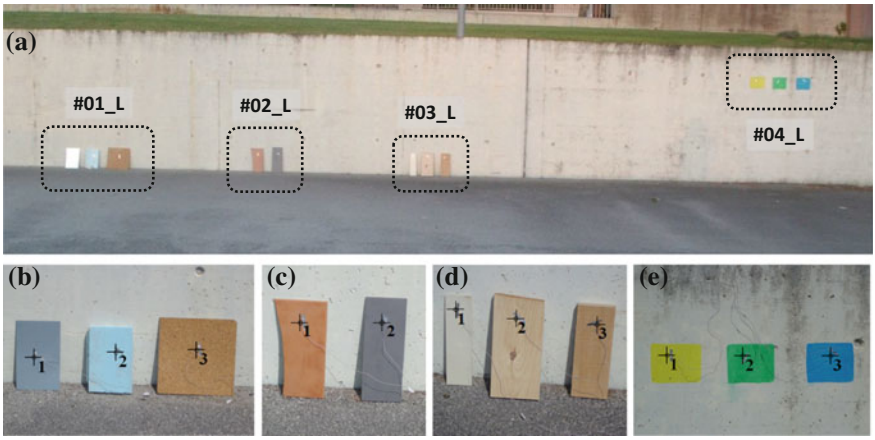

Fig. 2.4 Layout of the laboratory case study and location of the measuring points: **a** general view; **b** case study #01_L; **c** case study #02_L; **d** case study #03_L; **e** case study #04_L

- Case study #01_L consisted of three materials with low emissivity, "1" for a zinc plate, "2" for extruded polystyrene (XPS) and "3" for cork.
- Case study #02_L consisted of two ceramic tiles with different colours, "1" for an orange tile and "2" for a grey tile.
- Case study #03_L consisted of three types of wood, "1" for plywood, "2" for pine and "3" for beech.
- Case study #04_L: Three colours of a plastic paint were evaluated: "1" corresponding to yellow, "2" to green and "3" to blue.

Figure 2.4 shows the photographs of the four case studies of the laboratory campaign, including the exact location of the measuring points. Table 2.4 shows the environmental parameters used in the analysis of the thermal images and the emissivity values adopted for the materials.

The thermal images presented in this chapter were all obtained assuming a constant value of emissivity ($\varepsilon = 0.90$), for homogeneity purposes and to facilitate their comparison. Afterwards, in the image processing and analysis required to the determination of the surface temperature, the emissivity of each material was introduced as input. The values of emissivity were obtained in the literature, such as Gaussorgues (1999), Hart (2001) and Omega (2002).

Table 2.4 Emissivity, reflected temperature, air temperature and relative humidity for all laboratory case studies

		ε	Reflected temperature (°C)			Air temperature (°C)			Relative humidity (%)		
			(i)	(ii)	(iii)	(i)	(ii)	(iii)	(i)	(ii)	(iii)
#01_L	1	0.20	4.8	10.8	16.0	19.1	13.0	11.8	52.0	78.3	92.0
	2	0.60									
	3	0.70									
#02_L	1	0.93									
	2	0.93									
#03_L	1	0.83									
	2	0.90									
	3	0.94									
#04_L	1	0.93									
	2	0.92									
	3	0.94									

ε—Emissivity
(i)—Direct solar radiation; (ii)—after sunset; (iii)—during night-time

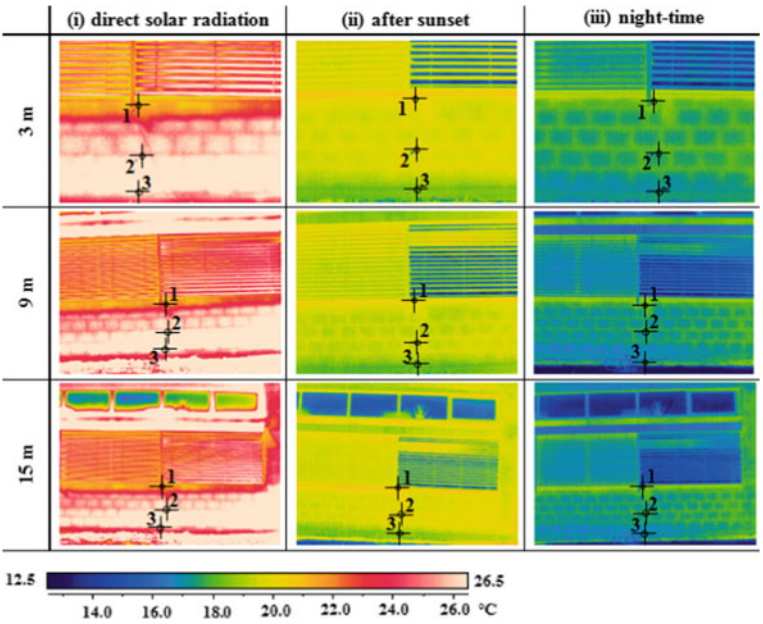

Fig. 2.5 Thermograms for case study #01_IS in the three periods of the day

2.3 Results of the In Situ Case Study

2.3.1 Case Study #01_IS

In Fig. 2.5, it is possible to observe the sequence of thermograms obtained throughout the test. In order to facilitate the interpretation and comparison of the thermal images, the same temperature scale was adopted for the entire data set.

Table 2.5 shows the results of the measurements carried out with the three devices, in the three periods of the day. The relative differences to the value measured by the thermocouple, assumed as the reference temperature, are also included in the table. To facilitate the interpretation of the differences, a colour scale (gradation) was included: blue for negative differences, white for null and red for positive differences.

Generally, the results show that there is no great difference between measurements made by the three devices. Even the effect of solar radiation did not prove to be very important, although the measurements made at 1:00 pm, with direct solar radiation, pointed out to slightly larger differences. The distance to the target was not an important factor as no clear relation was identified between this parameter and the relative differences between devices.

Table 2.5 Temperature results in case study #01_IS

Device	1			2			3		
	(i)	(ii)	(iii)	(i)	(ii)	(iii)	(i)	(ii)	(iii)
Thermocouple [°C]	22.7	20.1	17.2	27.8	20.3	18.1	25.3	18.7	17.7
Infrared thermometer [°C]	23.3	20.0	17.3	27.3	19.6	17.1	26.3	18.5	16.9
Thermogram at 3 m [°C]	22.2	19.9	17.7	26.7	19.8	17.8	24.1	18.3	17.1
Thermogram at 9 m [°C]	22.5	19.5	17.9	27.3	19.6	17.3	24.6	18.1	17.3
Thermogram at 15 m [°C]	22.3	20.0	17.9	27.3	19.6	17.2	24.2	18.4	17.3
Differences									
Infrared thermometer vs. thermocouple [°C]									
	0.6	-0.1	0.1	-0.5	-0.7	-1.0	1.0	-0.2	-0.8
Thermogram vs.thermocouple [°C]									
3 m	0.5	0.2	-0.5	1.1	0.5	0.3	1.2	0.4	0.6
9 m	0.2	0.6	-0.7	0.5	0.7	0.8	0.7	0.6	0.4
15m	0.4	0.1	-0.7	0.5	0.7	0.9	1.1	0.3	0.4
Infrared thermometer vs. thermogram [°C]									
3 m	1.1	0.1	-0.4	0.6	-0.2	-0.7	2.2	0.2	-0.2
9 m	0.8	0.5	-0.6	0.0	0.0	-0.2	1.7	0.4	-0.4
15 m	1.0	0.0	-0.6	0.0	0.0	-0.1	2.1	0.1	-0.4

2.3.2 Case Study #02_IS

In Fig. 2.6, it is possible to observe the sequence of thermograms obtained throughout the test. Once again, in order to facilitate the interpretation and comparison of the thermal images, the same temperature scale was adopted for the entire data set.

Table 2.6 shows the results of the measurements carried out with the three devices, in the three periods of the day, including the relative differences. To facilitate the interpretation of the results, the same colour scale used in case study #01_IS is applied once again.

Observing the results, the discrepancy of values obtained for point "3" is the most relevant finding. In fact, the measurements made with the IR camera are not very accurate. The high reflectance of this material, meaning that it is highly influenced by reflections, is the most likely reason to explain these results. The differences between the thermocouple and the infrared thermometer are relatively small, whichever the period of measurement. Once again, the distance to the target was not a relevant factor to explain the differences.

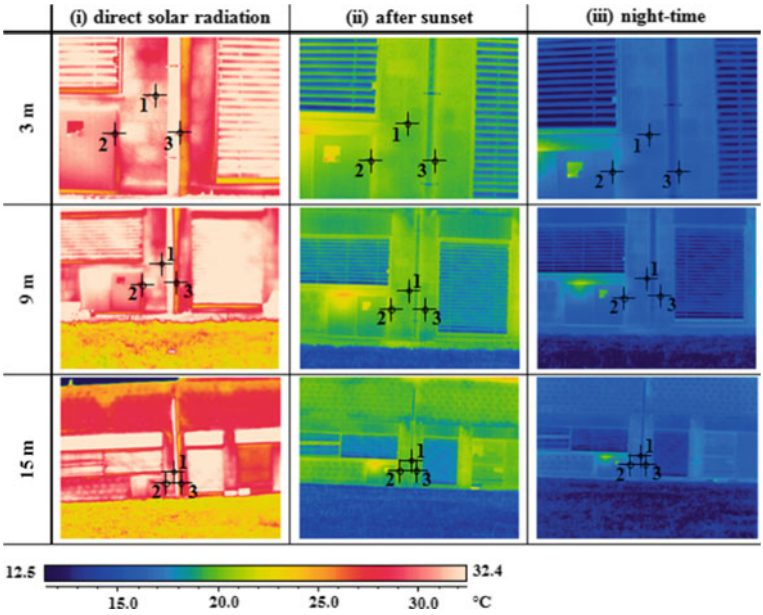

Fig. 2.6 Thermograms for case study #02_IS in the three periods of the day

2.3.3 Case Study #03_IS

Figure 2.7 shows the sequence of thermograms obtained throughout the test. In this case study, it was impossible to use the same temperature scale due to the high surface temperatures recorded in situation (i)—direct solar radiation. A different scale was thus used only for this period. The results of the measurements carried out with the three test devices, for the three periods of the day, as well as the relative differences between them, are displayed in Table 2.7.

The largest differences occur when the points are under direct solar radiation—scenario (i)—while in the other two periods the relative difference between devices is always below 2 °C. These results point out to the importance of, when quantitative thermography is intended, avoiding situations where radiation can be an important factor and thus bias the results. One should also stress the very good agreement between the infrared thermometer and thermograms after the sunset and at the night-time. As in the previous case studies, the distance to the target did not affect the accuracy of the measurements with the infrared camera.

Table 2.6 Temperature results in case study #02_IS

Device	1			2			3		
	(i)	(ii)	(iii)	(i)	(ii)	(iii)	(i)	(ii)	(iii)
Thermocouple [°C]	31.3	21.7	18.6	30.7	20.9	17.9	36.8	21.1	17.1
Infrared thermometer [°C]	32.9	20.7	17.5	32.5	20.6	17.7	35.5	20.6	16.7
Thermogram at 3 m [°C]	32.6	22.3	18.2	30.5	21.3	17.7	59.2	50.8	40.8
Thermogram at 9 m [°C]	32.5	22.3	18.0	30.3	21.3	17.6	57.8	50.5	40.8
Thermogram at 15 m [°C]	32.6	22.1	18.0	29.9	21.2	17.8	56.6	50.3	41.3
Differences									
Infrared thermometer vs. thermocouple [°C]									
	1.6	-1.0	-1.1	1.8	-0.3	-0.2	-1.3	-0.5	-0.4
Thermogram vs.thermocouple [°C]									
3 m	-1.3	-0.6	0.4	0.2	-0.4	0.2	-22.4	-29.7	-23.7
9 m	-1.2	-0.6	0.6	0.4	-0.4	0.3	-21.0	-29.4	-23.7
15 m	-1.3	-0.4	0.6	0.8	-0.3	0.1	-19.8	-29.2	-24.2
Infrared thermometer vs. thermogram [°C]									
3 m	0.3	-1.6	-0.7	2.0	-0.7	0.0	-23.7	-30.2	-24.1
9 m	0.4	-1.6	-0.5	2.2	-0.7	0.1	-22.3	-29.9	-24.1
15 m	0.3	-1.4	-0.5	2.6	-0.6	-0.1	-21.1	-29.7	-24.6

2.3.4 Case Study #04_IS

Figures 2.8 and 2.9 depict the sequence of thermograms obtained throughout the test. The sequence of thermograms presented for both test angles is on the same temperature scale. Table 2.8 shows the results of the measurements carried out with the three devices, in the three periods of the day and for the two angles between the IR camera and the target, including the relative differences.

The inaccuracy in the measurement of the surface temperature of metallic elements with the IR camera is once again evident as the relative differences in point "2" are always higher than 6 °C, reaching 18 °C under direct solar radiation and for α1. Regarding the angle between the IR camera and the target, the first angle, α1, presented a better performance after the sunset and during night-time, while the opposite situation occurred when the specimen was under direct solar radiation. This situation confirms, once more, the importance of solar radiation in quantitative thermography. As in the previous examples, no clear trend was identified concerning the distance to the target.

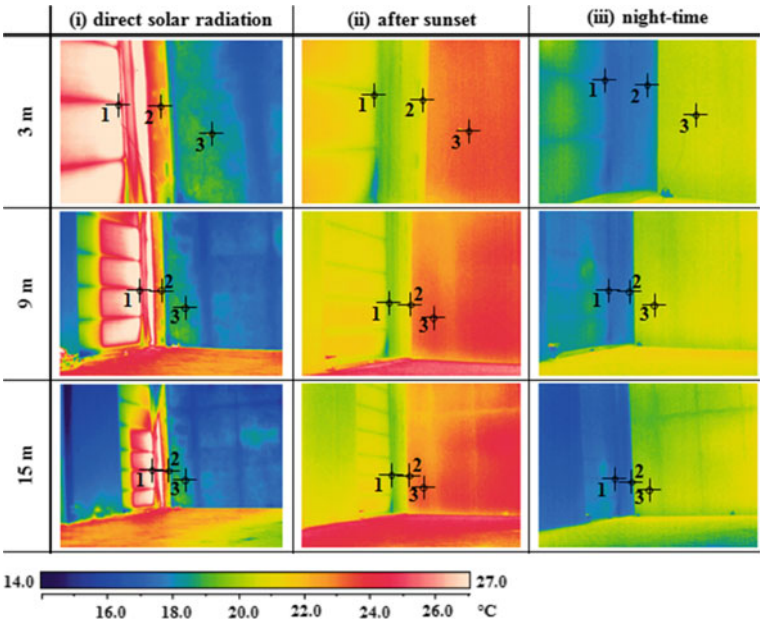

Fig. 2.7 Thermograms for case study #03_IS in the three periods of the day (temperature scale only for (ii) and (iii))

2.4 Results of the Laboratory Case Study

2.4.1 Case Study #01_L

In Fig. 2.10, it is possible to observe the sequence of thermograms obtained throughout the test. All the thermograms are presented with the same temperature scale. Table 2.9 shows the results of the measurements carried out with the three devices, in the three periods of the day, including the relative differences. To facilitate the interpretation of the results, a colour scale used is applied once again: blue for negative differences, white for null and red for positive differences.

The results show that the surface temperature measured by the infrared thermometer and the infrared camera is not accurate for the zinc plate, regardless of the time of the day and the distance. This is related to reflections, as metallic surfaces have very high reflectance, which considerably influences the results. Overall, the smallest differences occurred in the measurements made during night-time. However, the results reveal that the surface temperature measured under direct solar radiation can be quite different, even if measured with the same equipment, which was expected as the materials have different thermal properties.

Table 2.7 Temperature results in case study #03_IS

Device	1			2			3		
	(i)	(ii)	(iii)	(i)	(ii)	(iii)	(i)	(ii)	(iii)
Thermocouple [°C]	50.5	20.6	17.9	46.2	20.8	17.9	35.8	23.8	21.1
Infrared thermometer [°C]	52.1	21.3	18.4	46.9	21.2	18.0	36.9	24.1	21.0
Thermogram at 3 m [°C]	53.0	20.6	17.8	45.4	21.2	18.1	36.9	23.9	21.2
Thermogram at 9 m [°C]	53.0	20.4	17.7	45.4	21.2	18.1	36.9	23.9	21.1
Thermogram at 15 m [°C]	53.1	20.5	17.6	45.3	21.2	18.0	37.0	23.6	20.7
Differences									
Infrared thermometer vs. thermocouple [°C]									
	1.6	0.7	0.5	0.7	0.4	0.1	1.1	0.3	-0.1
Thermogram vs.thermocouple [°C]									
3 m	-2.5	0.0	0.1	0.8	-0.4	-0.2	-1.1	-0.1	-0.1
9 m	-2.5	0.2	0.2	0.8	-0.4	-0.2	-1.1	-0.1	0.0
15 m	-2.6	0.1	0.3	0.9	-0.4	-0.1	-1.2	0.2	0.4
Infrared thermometer vs. thermogram [°C]									
3 m	-0.9	0.7	0.6	1.5	0.0	-0.1	0.0	0.2	-0.2
9 m	-0.9	0.9	0.7	1.5	0.0	-0.1	0.0	0.2	-0.1
15 m	-1.0	0.8	0.8	1.6	0.0	0.0	-0.1	0.5	0.3

The distance from the camera to the target also seems to influence the results, generally decreasing surface temperature. As the distance is less than 10 m, differences between the measurements were not expected (Chew 1998). One possible reason derives from the samples being on the ground in a position with a slight bias from perpendicular.

2.4.2 Case Study #02_L

In Fig. 2.11, it is possible to observe the sequence of thermograms obtained throughout the test. All the thermograms are presented with the same temperature scale. Table 2.10 shows the results of the measurements carried out with the three devices, in the three periods of the day, including the relative differences.

The most accurate results were, once again, obtained during night-time, while the largest differences occurred in period (i)—direct solar radiation. In this case study, it was also possible to identify a direct relationship between the relative differences and the distance to the target, regardless of the period of the day. As expected, no significant differences were attained between the orange and the grey tile. However, when the measurements are carried out with direct solar radiation, the grey tile

Table 2.8 Temperature results in case study #04_IS

Device	1			2			3		
	(i)	(ii)	(iii)	(i)	(ii)	(iii)	(i)	(ii)	(iii)
Thermocouple [°C]	36.7	24.2	20.6	35.7	23.6	20.1	37.5	22.9	19.5
Infrared thermometer [°C]	30.2	25.3	21.1	32.8	23.7	20.4	33.4	23.1	19.4
Thermograms for α1 [°C]									
Thermogram at 3 m [°C]	32.9	25.4	21.4	17.4	30.3	28.6	36.8	22.9	19.5
Thermogram at 9 m [°C]	33.0	25.0	21.5	18.2	30.9	28.3	37.0	22.6	19.2
Thermogram at 15 m [°C]	32.9	24.9	21.1	18.3	30.9	30.0	37.1	22.7	19.2
Thermograms for α2 [°C]									
Thermogram at 3 m [°C]	33.1	26.1	21.1	23.6	42.4	33.5	35.4	23.3	18.8
Thermogram at 9 m [°C]	33.2	26.0	22.2	24.0	42.3	36.1	35.6	23.0	19.7
Thermogram at 15 m [°C]	33.1	26.0	22.2	23.2	42.5	36.1	36.2	22.8	19.8
Differences									
Infrared thermometer vs. thermocouple [°C]									
	-6.5	1.1	0.5	-2.9	0.1	0.3	-4.1	0.2	-0.1
Thermogram vs.thermocouple for α1 [°C]									
3 m	3.8	-1.2	-0.8	18.3	-6.7	-8.5	0.7	0.0	0.0
9 m	3.7	-0.8	-0.9	17.5	-7.3	-8.2	0.5	0.3	0.3
15 m	3.8	-0.7	-0.5	17.4	-7.1	-9.9	0.4	0.2	0.3
Thermogram vs.thermocouple for α2 [°C]									
3 m	3.6	-1.9	-0.5	12.1	-18.8	-13.4	2.1	-0.4	0.7
9 m	3.5	-1.8	-1.6	11.7	-18.7	-16.0	1.9	-0.1	-0.2
15 m	3.6	-1.8	-1.6	12.5	-18.9	-16.0	1.3	0.1	-0.3
Infrared thermometer vs. thermogram for α1 [°C]									
3 m	-2.7	-0.1	-0.3	15.4	-6.6	-8.2	-3.4	0.2	-0.1
9 m	-2.8	0.3	-0.4	14.6	-7.2	-7.9	-3.6	0.5	0.2
15 m	-2.7	0.4	0.0	14.5	-7.0	-9.6	-3.7	0.4	0.2
Infrared thermometer vs. thermogram for α2 [°C]									
3 m	-2.9	-0.8	0.0	9.2	-18.7	-13.1	-2.0	-0.2	0.6
9 m	-3.0	-0.7	-1.1	8.8	-18.6	-15.7	-2.2	0.1	-0.3
15 m	-2.9	-0.7	-1.1	9.6	-18.8	-15.7	-2.8	0.3	-0.4

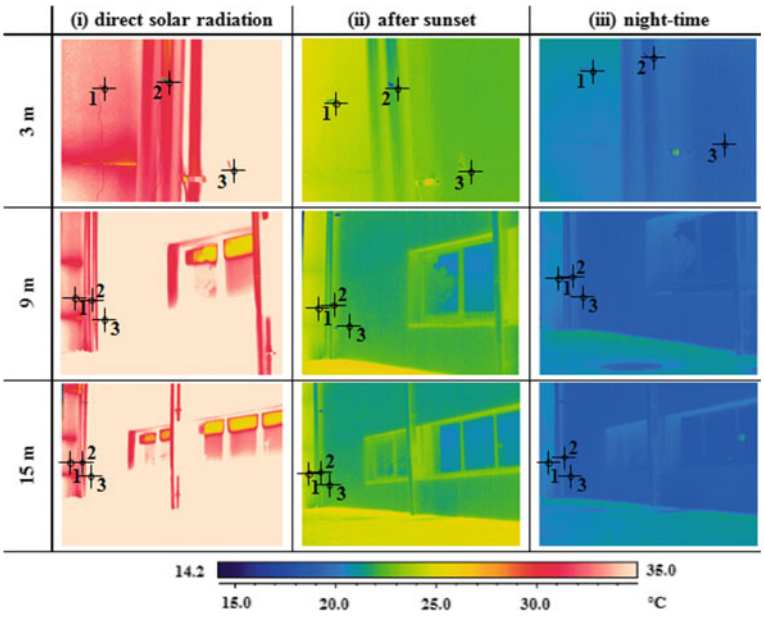

Fig. 2.8 Thermograms for case study #04_IS and for α1 in the three periods of the day

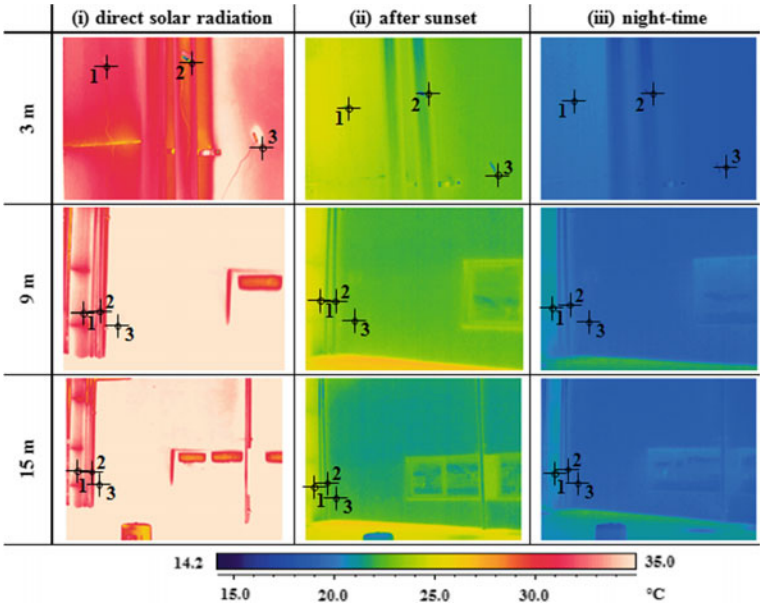

Fig. 2.9 Thermograms for case study #04_IS and for α2 in the three periods of the day

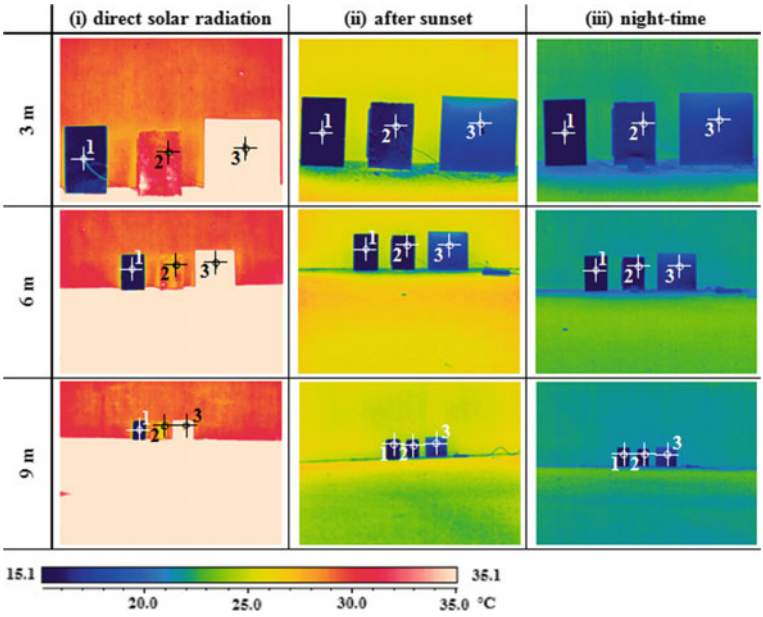

Fig. 2.10 Thermograms for case study #01_L in the three periods of the day

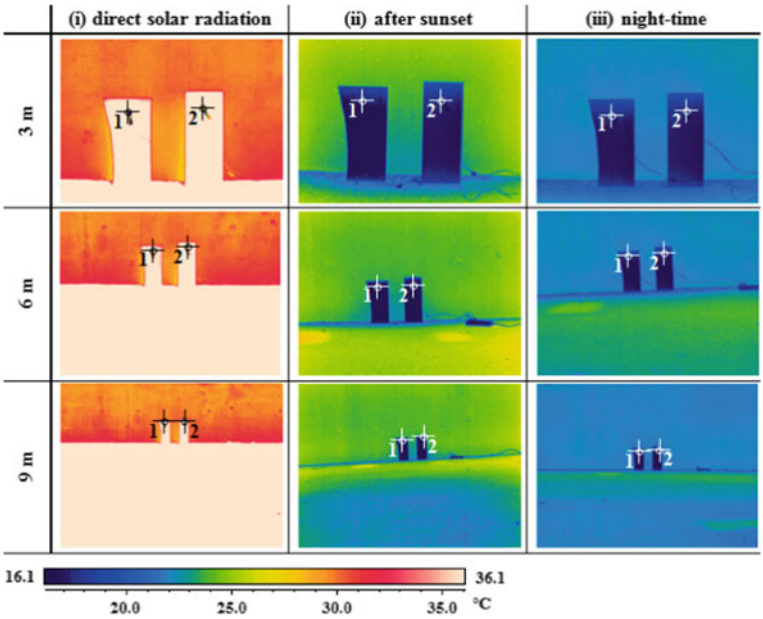

Fig. 2.11 Thermograms for case study #02_L in the three periods of the day

Table 2.9 Temperature results in case study #01_L

Device	1			2			3		
	(i)	(ii)	(iii)	(i)	(ii)	(iii)	(i)	(ii)	(iii)
Thermocouple [°C]	47.1	18.4	17.3	40.3	17.6	16.2	44.1	18.2	18.4
Infrared thermometer [°C]	37.2	15.3	16.7	35.7	14.6	16.9	46.4	16.4	17.8
Thermogram at 3 m [°C]	52.2	-39.1	-4.8	42.2	17.9	16.9	45.8	21.7	18.2
Thermogram at 6 m [°C]	15.2	-40.1	-9.6	40.1	15.9	15.9	46.6	20.8	17.7
Thermogram at 9 m [°C]	-40.1	-40.1	-13.5	38.3	14.5	14.8	44.7	19.6	17.3
Differences									
Infrared thermometer vs. thermocouple [°C]									
	-9.9	-3.1	-0.6	-4.6	-3.0	0.7	2.3	-1.8	-0.6
Thermogram vs.thermocouple [°C]									
3 m	-5.1	57.5	22.1	-1.9	-0.3	-0.7	-1.7	-3.5	0.2
6 m	31.9	58.5	26.9	0.2	1.7	0.3	-2.5	-2.6	0.7
9 m	87.2	58.5	30.8	2.0	3.1	1.4	-0.6	-1.4	1.1
Infrared thermometer vs. thermogram [°C]									
3 m	-15.0	54.4	21.5	-6.5	-3.3	0.0	0.6	-5.3	-0.4
6 m	22.0	55.4	26.3	4.4	1.3	1.0	-0.2	-4.4	0.1
9 m	77.3	55.4	30.2	-2.6	0.1	2.1	1.7	-3.2	0.5

presents slightly higher temperatures, while when measurements are performed after sunset and during night-time, the surface temperature is very similar in the two specimens.

2.4.3 Case Study #03_L

In Fig. 2.12, it is possible to observe the sequence of thermograms obtained throughout the test. All the thermograms are presented with the same temperature scale. Table 2.11 shows the results of the measurements carried out with the three devices, in the three periods of the day, including the relative differences.

The results confirm the negative effect of direct solar radiation, as the relative differences were always higher in this period, regardless of the material. The highest relative differences occurred between the thermocouple and thermograms. However ,

Table 2.10 Temperature results in case study #02_L

Device	1			2		
	(i)	(ii)	(iii)	(i)	(ii)	(iii)
Thermocouple [°C]	43.9	19.1	17.8	46.9	19.0	17.6
Infrared thermometer [°C]	42.2	17.9	17.4	43.3	17.9	17.4
Thermogram at 3 m [°C]	40.4	17.8	17.6	41.2	17.8	17.5
Thermogram at 6 m [°C]	39.5	16.0	17.3	41.0	16.1	17.2
Thermogram at 9 m [°C]	37.8	15.7	17.1	39.5	15.7	16.8
Differences						
Infrared thermometer vs. thermocouple [°C]						
	-1.7	-1.2	-0.4	-3.6	-1.1	-0.2
Thermogram vs.thermocouple [°C]						
3 m	3.5	1.3	0.2	5.7	1.2	0.1
6 m	4.4	3.1	0.5	5.9	2.9	0.4
9 m	6.1	3.4	0.7	7.4	3.3	0.8
Infrared thermometer vs. thermogram [°C]						
3 m	1.8	0.1	-0.2	2.1	0.1	-0.1
6 m	2.7	1.9	0.1	2.3	1.8	0.2
9 m	4.4	2.2	0.3	3.8	2.2	0.6

generally, the differences are smaller when compared with the ones obtained in the case studies #01_L and #02_L. Besides, by contrast with these two cases, the distance from the camera to the target is not so relevant, possibly due to the thermal/optical properties of the wood.

2.4.4 Case Study #04_L

In Fig. 2.13, it is possible to observe the sequence of thermograms obtained throughout the test. All the thermograms are presented with the same temperature scale. Table 2.12 shows the results of the measurements carried out with the three devices, in the three periods of the day, including the relative differences. The measurements performed by the different devices are very similar. The largest differences occurred in colour blue under direct solar radiation.

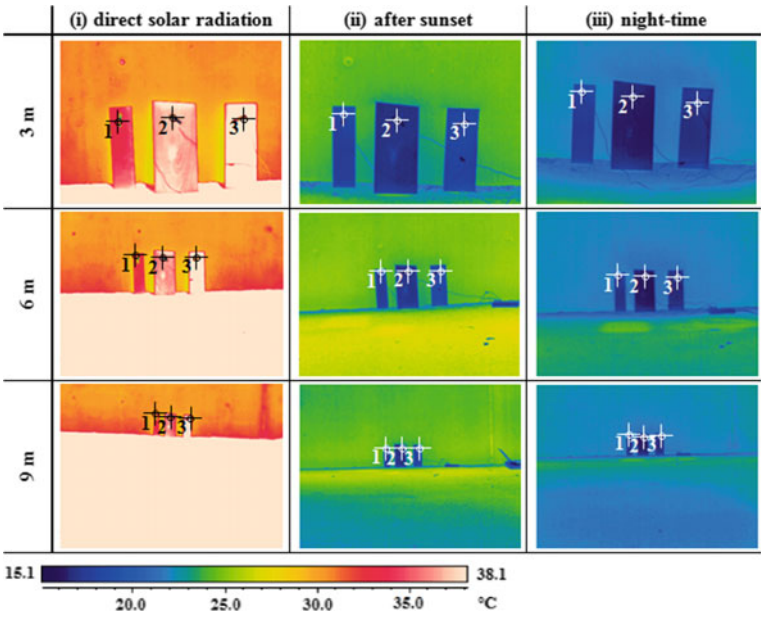

Fig. 2.12 Thermograms for case study #03_L in the three periods of the day

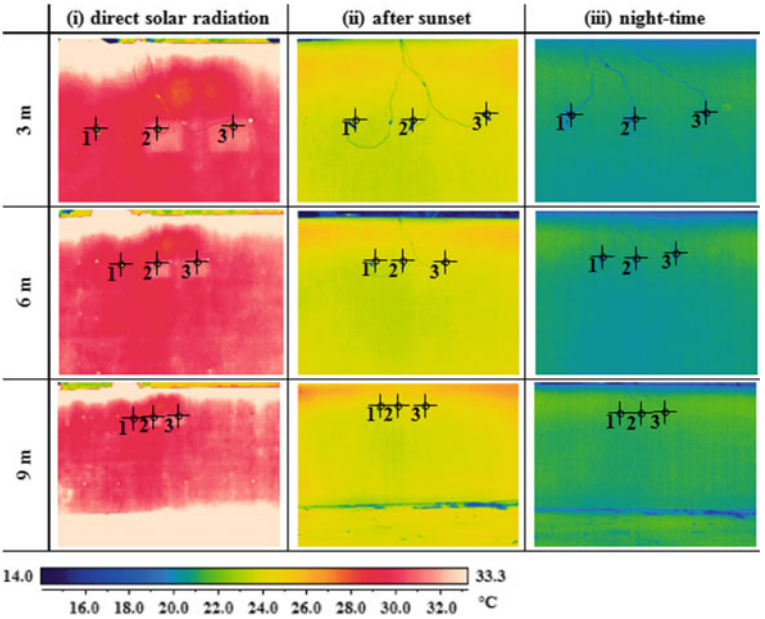

Fig. 2.13 Thermograms for case study #04_L in the three periods of the day

Table 2.11 Temperature results in case study #03_L

Device	1			2			3		
	(i)	(ii)	(iii)	(i)	(ii)	(iii)	(i)	(ii)	(iii)
Thermocouple [°C]]	37.7	18.7	18.0	41.7	18.1	16.6	43.3	18.9	18.8
Infrared thermometer [°C]	36.6	17.9	18.1	39.4	17.6	16.9	41.7	18.4	17.4
Thermogram at 3 m [°C]	38.2	18.0	18.7	39.7	17.7	16.8	41.1	18.9	17.4
Thermogram at 6 m [°C]	37.3	17.9	18.3	39.3	17.8	16.6	41.3	19.2	17.3
Thermogram at 9 m [°C]	36.9	17.3	18.4	38.9	17.7	16.7	39.4	19.0	17.5
Differences									
Infrared thermometer vs. thermocouple [°C]									
	-1.1	-0.8	0.1	-2.3	-0.5	0.3	-1.6	-0.5	-1.4
Thermogram vs.thermocouple [°C]									
3 m	-0.5	0.7	-0.7	2.0	0.4	-0.2	2.2	0.0	1.4
6 m	0.4	0.8	-0.3	2.4	0.3	0.0	2.0	-0.3	1.5
9 m	0.8	1.4	-0.4	2.8	0.4	-0.1	3.9	-0.1	1.3
Infrared thermometer vs. thermogram [°C]									
3 m	-1.6	-0.1	-0.6	-0.3	-0.1	0.1	0.6	-0.5	0.0
6 m	-0.7	0.0	-0.2	0.1	-0.2	0.3	0.4	-0.8	0.1
9 m	-0.3	0.6	-0.3	0.5	-0.1	0.2	2.3	-0.6	-0.1

2.5 Discussion of the Results

In the experimental campaign described in this chapter, several set-ups and boundary conditions were created to compare the performance of IRT with other surface temperature measurement techniques such as infrared thermometer and thermocouples. The main objective was to understand the ideal conditions for accurate measurements with the infrared camera.

The most evident finding of the tests was the fact that the surface temperature measured under direct solar radiation can be very tricky. In fact, the results show different surface temperatures even when measured with the same device. After sunset and at night-time, the differences are lower as the sun is not influencing the measurements.

The results also show that the surface temperature measured by the infrared thermometer and the infrared camera is not accurate for metallic materials with low emissivity, regardless of the time of the day and the distance to the target. The most probable reason for this is the effect of reflections, as metallic surfaces have very high reflectance, which considerably influences the results.

Table 2.12 Temperature results in case study #04_L

Device	1			2			3		
	(i)	(ii)	(iii)	(i)	(ii)	(iii)	(i)	(ii)	(iii)
Thermocouple [°C]]	30.9	24.3	21.8	32.6	24.5	21.4	33.6	24.7	21.5
Infrared thermometer [°C]	31.6	24.1	20.7	33.2	24.2	21.1	32.8	24.5	21.3
Thermogram at 3 m [°C]	31.4	24.3	21.0	32.6	24.7	21.2	32.2	24.8	21.1
Thermogram at 6 m [°C]	31.4	24.1	21.1	32.7	24.6	21.2	32.2	24.7	20.9
Thermogram at 9 m [°C]	31.2	24.4	21.4	32.7	25.0	21.2	31.8	24.9	21.6
Differences									
Infrared thermometer vs. thermocouple [°C]									
	0.7	-0.2	-1.1	0.6	-0.3	-0.3	-0.8	-0.2	-0.2
Thermogram vs.thermocouple [°C]									
3 m	-0.5	0.0	0.8	0.0	-0.2	0.2	1.4	-0.1	0.4
6 m	-0.5	0.2	0.7	-0.1	-0.1	0.2	1.4	0.0	0.6
9 m	-0.3	-0.1	0.4	-0.1	-0.5	0.2	1.8	-0.2	-0.1
Infrared thermometer vs. thermogram [°C]									
3 m	0.2	-0.2	-0.3	0.6	-0.5	-0.1	0.6	-0.3	0.2
6 m	0.2	0.0	-0.4	0.5	-0.4	-0.1	0.6	-0.2	0.4
9 m	0.4	-0.3	-0.7	0.5	-0.8	-0.1	1.0	-0.4	-0.3

Concerning the laboratory case studies, the average absolute error (excluding the zinc plate) was 5.6%. The measurements performed during the night are the most accurate ones, as the values obtained by the infrared devices are quite similar to the ones measured by the thermocouples (an error of 2.7% on average). The more accurate set-up was the infrared camera with a distance to the target of 3.0 m. The distance to the target also influences the results, generally decreasing surface temperature and increasing the error up to 7.2%. That may be related not only with the distance to the target but also because the samples were on the ground in a position with a slight bias from perpendicular.

References

Avdelidis N, Moropoulou A (2003) Emissivity considerations in building thermography. Energy Buildings 35(7):663–667

Barreira E, Freitas VP (2007) Evaluation of building materials using infrared thermograph. Construction Building Mater 21(1):218–224

Chew M (1998) Assessing building façades using infra-red thermography. Struct Survey 16(2):81–86
Gaussorgues G (1999) La thermographie infrarouge—Principes, technologies, applications. 4.e Édition. Paris, Edition TEC & DOC
Hart J (2001) A practical guide for infra-red thermography for building surveys. BRE, UK
Omega (2002) Transactions vol 1—non-contact temperature measurement, 2nd edn. Putman Publishing Company and Omega Press LLC

Chapter 3
IRT Versus Moisture: Laboratory Tests

3.1 Aim

Several authors have used IRT to assess moisture (Balaras and Argiriou 2002; Avdelidis et al. 2003; Edis et al. 2014; Menezes et al. 2015); nevertheless, it is of most interest to evaluate its applicability in the laboratory, under controlled conditions, using full-scale models. Two situations were assessed: moisture intake due to rising damp and the drying process of a moist surface. In both cases, the passive approach was implemented as no external heat source was used. Moist areas were detected due to the effect of evaporative cooling at the surface.

A wall made of limestone blocks was selected as a case study to assess rising damp. The specimen was partially immersed in water for about 3 weeks, and thermal images were taken before and during the absorption period. To assess the drying process of a moist surface, a typical brick wall covered with painted rendering was sprayed with water on a limited area and thermal images were taken during the drying period, which lasted about 10 days. For the two phenomena, besides thermal images, a moisture detector was also used to qualitatively evaluate the moisture content of the walls.

3.2 Materials and Techniques

3.2.1 Set-up and Methodology

A full-scale limestone wall was used to assess raising damp. The specimen was partially immersed in 0.35 m of water for about 3 weeks. Measurements on the central area of the specimen (Fig. 3.1a) were carried out before the immersion period began (0 h) and 2, 4, 8, 28, 52, 100, 148, 196, 268, 340 and 532 h after the immersion.

E. Barreira and R. M. S. F Almeida, *Infrared Thermography for Building Moisture Inspection*, SpringerBriefs in Applied Sciences and Technology,
https://doi.org/10.1007/978-3-319-75386-7_3

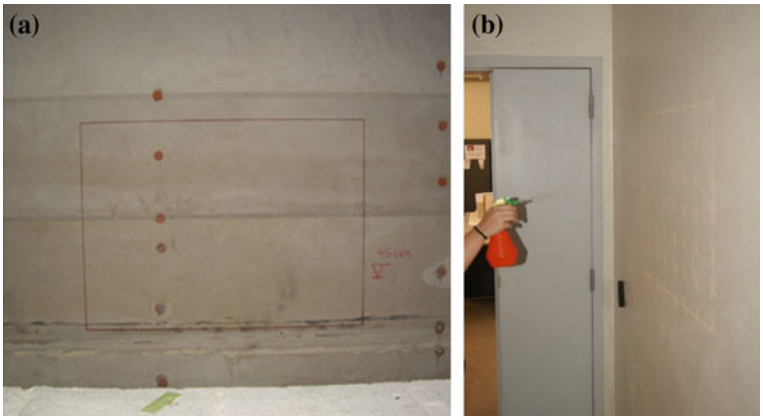

Fig. 3.1 **a** Area of the limestone wall used to assess rising damp; **b** area of the brick wall covered with painted rendering used to assess the drying process

A typical brick wall covered with painted rendering was used to assess the drying process of a moist surface. A limited area of the wall was sprayed three times with about 3 ml of water. The drying period took about 10 days. Measurements were carried out before spraying the surface, immediately after and every 15 min in the first hour. Additional measurements were also carried out 4, 28, 124 and 244 h after spraying the surface (Fig. 3.1b).

The measurements were performed using an IR camera, to assess the thermal patterns, and a moisture detector, to evaluate the relative moisture content of the walls. Throughout both tests, the IR camera was always kept in the same position. Average temperature and relative humidity in the laboratory during the test period were around 19 °C and 70%, respectively.

The moisture level above the water plan was also measured (stained/wet area), whenever the thermal images and the measurements with the moisture detector were carried out.

To compare the thermal images with the results of the moisture detector, a colour scale was proposed for the results of the detector. The warmer colours in the thermal image were linked to the lower values of the detector relative scale because in the dryer areas evaporation is less intense and therefore the surface temperature is higher (Fig. 3.2).

As the moisture detector only allows spot measurements and to guarantee a reliable comparison between the 2D thermal images and the results of the moisture detector, the area under study was divided into a grid. When assessing rising damp, the grid area was 0.78×0.45 m^2 and a total of 30 points were defined (Fig. 3.3a). To assess the drying process, the grid area was 0.70×0.60 m^2 and a total of 56 points were defined (Fig. 3.3b). Using the values measured at each point and the colour scale, a surface graph was created.

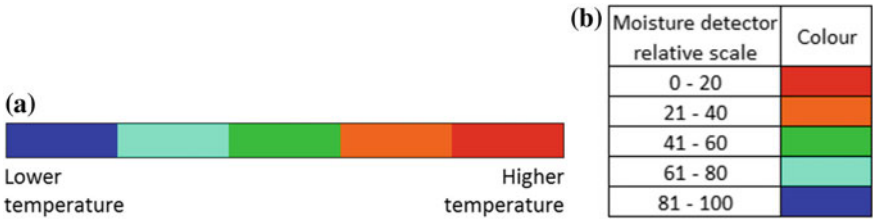

Fig. 3.2 **a** Thermal images colour scale (temperature in ºC); **b** relative scale of the moisture detector and the corresponding colour scale

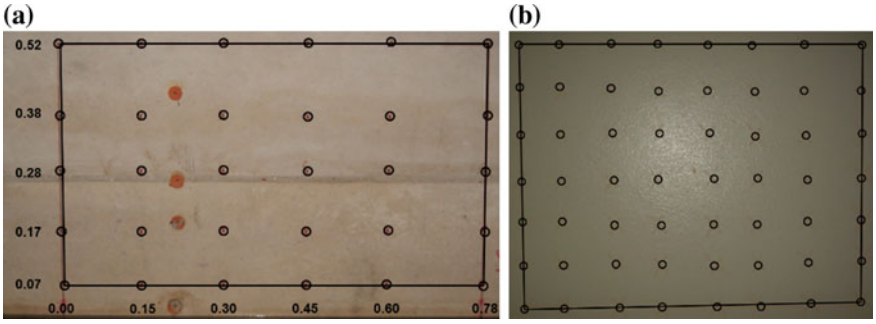

Fig. 3.3 **a** Grid of the area under study when assessing rising damp; **b** grid of the area under study when assessing the drying process

3.2.2 Equipment

Two different devices were used in this research: infrared camera (Fig. 3.4a) and moisture detector (Fig. 3.4b). The main specifications of the infrared camera are described in Table 3.1. The moisture detector is a non-destructive equipment that operates on the principle that the electrical impedance of a material varies in proportion to its moisture content. The instrument measures the electrical impedance of a material by creating a low-frequency alternating electric field between the electrodes. The reading displayed by the equipment is a relative scale in percentage, which indicates the greater or lesser signal (lower values indicate lesser signal that corresponds to lower moisture content).

Before the measurements were carried out, the calibration procedures were performed according to the operation manual of each device. Reflection calibration and ambient and background compensation of the infrared camera were assessed before each measurement.

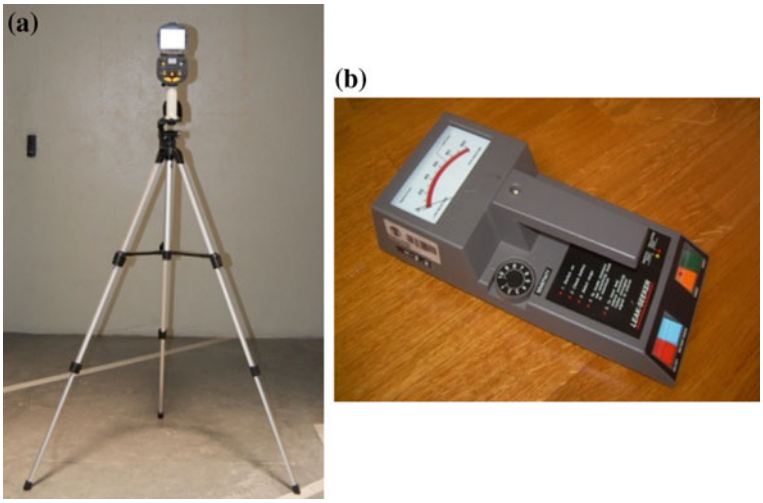

Fig. 3.4 Devices: **a** Infrared camera; **b** moisture detector

Table 3.1 Specifications of infrared camera

	Infrared camera
Measuring range	−20 to 100 °C
Resolution	0.1 °C
Accuracy	±2 °C or ±2% of reading
Detector	Uncooled focal plane array (microbolometer)
Spectral range	8–14 μm
Thermal image pixels	320 (H) × 240 (V) pixels
Focusing range	50 cm to infinite
IFOV	1.5 mrad

3.2.3 Materials

The dimensions of the limestone wall are $2.00 \times 1.85 \times 0.20$ m^3, and it is composed of six blocks with 0.30 m height with horizontal mortar joints of about 1 cm thick (Fig. 3.1). The brick wall was covered with a cement-based plaster and finished with light coloured paint. The properties of the materials used in the models are presented in Table 3.2. More information about this specimen can be found in Guimarães et al. 2010.

Table 3.2 Properties of the materials used in the models

Material	ε (−)	λ (W/m K)	ρ (kg/m^3)	c (J/kg K)
Limestone	0.88	0.723	2500	840
Mortar	0.93	1.37	1685	1000
Brick	0.86	0.60	1800	850
Paint	0.90	–		–

3.3 Results

3.3.1 Moisture Caused by Rising Damp

For evaluating rising damp, the highest visible moisture level above the water plan was measured, whenever thermal images were taken and moisture content was measured. Figure 3.5 shows the time variation of the highest visible moisture level above the water plan. A fast increase in the highest visible moisture level is visible in the first 240 h, and afterwards, it remained approximately constant until the end of the test. The stabilization occurred due to the equilibrium between the water intake and the evaporation at the surface.

Figures 3.6, 3.7, 3.8, 3.9, 3.10, 3.11, 3.12, 3.13 and 3.14 show the evolution of the moisture level in the specimen during the entire period of absorption (532 h) using both the thermal images and the results of the moisture detector. Both the thermal image and the measurement with the moisture detector show that the specimen was dry before the humidification started (Fig. 3.6). Immediately after the tank was filled with water (0.35 m of water above the bottom plan of the specimen), the water plan can be detected in the thermal image as a colder area, limited by the black line in the image (Fig. 3.7).

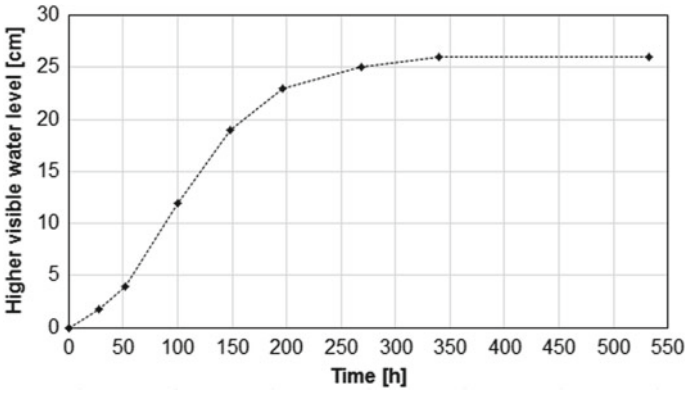

Fig. 3.5 Time variation of the highest visible moisture level above the water plan

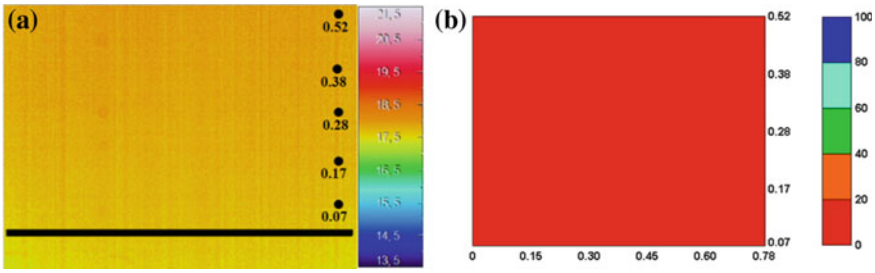

Fig. 3.6 Measurements before immersion began: **a** thermal image; **b** moisture detector results

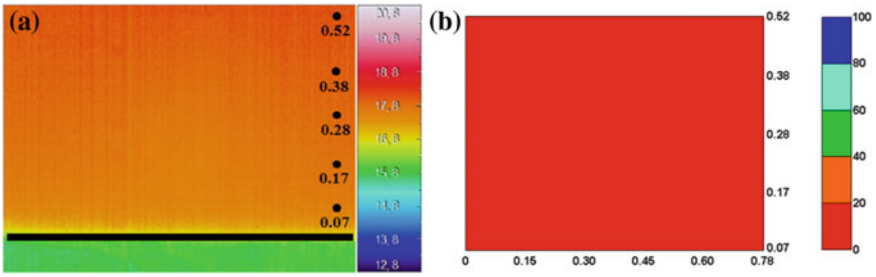

Fig. 3.7 Measurements immediately after the humidification began: **a** thermal image; **b** moisture detector results

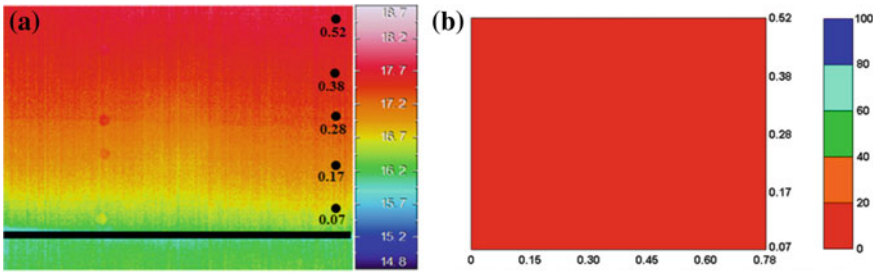

Fig. 3.8 Measurements 52 h after the imbibition began: **a** thermal image; **b** moisture detector results

At $t = 52$ h (Fig. 3.8), the highest moisture level above the water plan is about 0.04 m (Fig. 3.5), corresponding to the top of the green isothermal (Fig. 3.8a). The yellow isothermal shows the transition area between the wet and dry surfaces of the specimen. With the moisture detector (Fig. 3.8b), the rising damp was not identified yet because the moisture level has not reached the first row of the grid (0.07 m). About 2 days later, at $t = 100$ h, the thermal image shows that the top of the green isotherm is between the levels 0.07 and 0.17 m (Fig. 3.9a). This is supported both by the results of the moisture detector (Fig. 3.9b) and by the highest visible moisture level (Fig. 3.5).

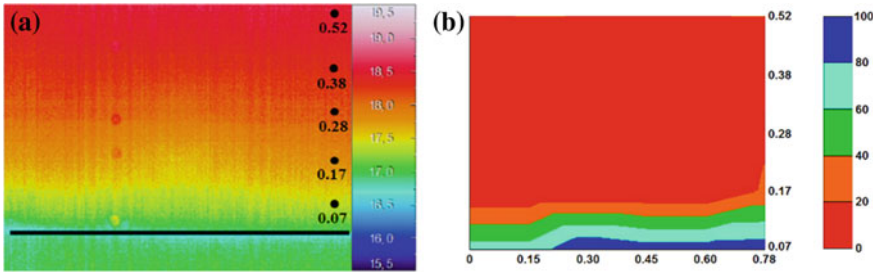

Fig. 3.9 Measurements 100 h after the imbibition began: **a** thermal image; **b** moisture detector results

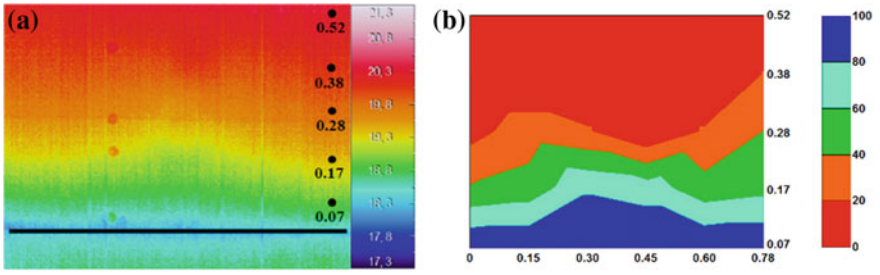

Fig. 3.10 Measurements 148 h after the imbibition began: **a** thermal image; **b** moisture detector results

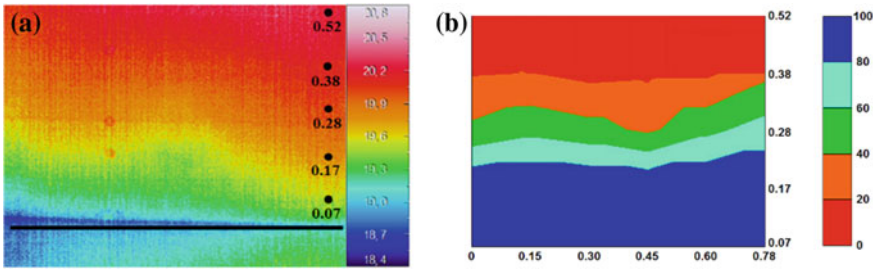

Fig. 3.11 Measurements 196 h after the imbibition began: **a** thermal image; **b** moisture detector results

Figures 3.10, 3.11, 3.12, 3.13 and 3.14 show that the thermal images point in the same direction as the results obtained with the moisture detector. Indeed, the moisture level assessed by both methods is quite similar. The thermal images also show that the moisture level is higher in the centre of the specimen and lower near the verticals corners, which was not visually perceptible. This phenomenon can be explained by the effect of more intense rising damp evaporation near the corners of the specimen.

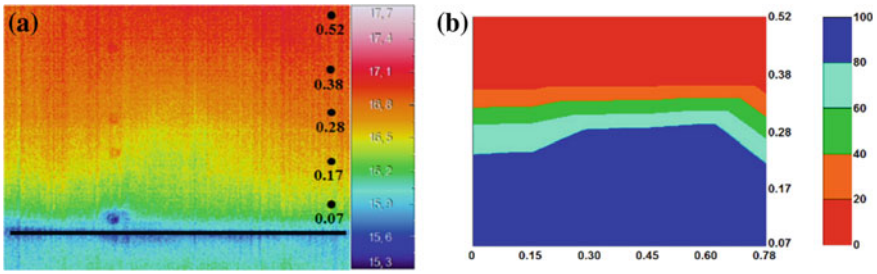

Fig. 3.12 Measurements 268 h after the imbibition began: **a** thermal image; **b** moisture detector results

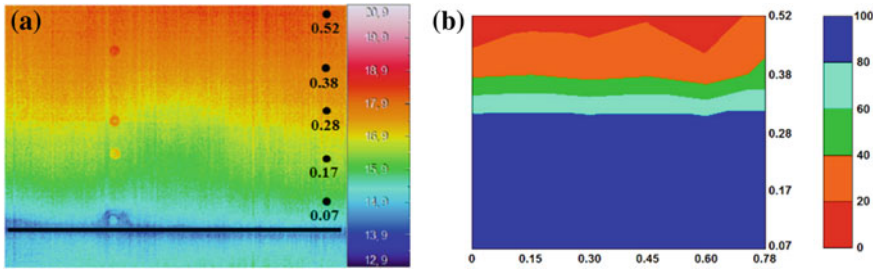

Fig. 3.13 Measurements 340 h after the imbibition began: **a** thermal image; **b** moisture detector results

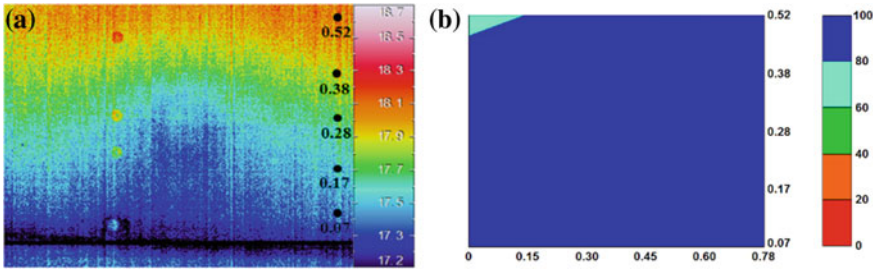

Fig. 3.14 Measurements 532 h after the imbibition began: **a** thermal image; **b** moisture detector results

At the end of the measurement, the results of the moisture detector (Fig. 3.14b) show that the level of the moist area (dark blue) is above 0.52 m, while in the thermal image (Fig. 3.14a), it is around 0.38 m. Also, the difference between the thermal images in Figs. 3.13a and 3.14a are not very relevant, pointing to a stabilization of the moisture level. On the other hand, when analysing the results of the moisture detector, a more pronounced difference can be found. Although these results are not completely in accordance, they are expectable. In fact, IRT only detects surface evaporation and the moisture detector assesses inner moist (around 2 cm penetration

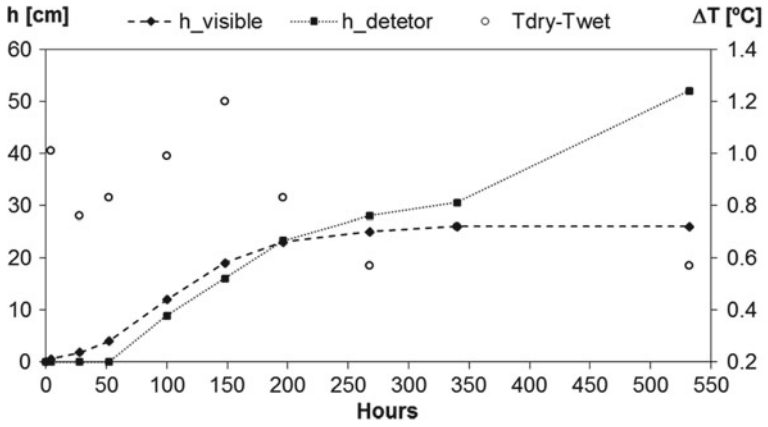

Fig. 3.15 Time variation of the highest visible moisture level above the water plan (h_visible), the highest moisture level above the water plan measured by the moisture detector (h_detector) and the temperature difference between the dry and wet areas (Tdry-Twet)

depth). This is also in line with the results of the numerical simulation performed by Guimarães et al. (2010), showing that the moisture level at the surface is lower than inside the specimen, because evaporation is more preponderant than capillarity, which allows the stabilization of the superficial moisture level. Inside the specimen, capillarity remains the main driving force and the moisture level keeps increasing.

Figure 3.15 shows the time variation of the highest visible moisture level above the water plan (h_visible), the highest moisture level above the water plan measured by the moisture detector (h_detector) and the temperature difference between the dry and wet areas (Tdry-Twet) calculated from the thermal images. The results indicate that the temperature difference increases until 148 h after the start of the humidification and then decreases, becoming stable after approximately 268 h, with a value around 0.6 °C. The temperature gradient starts decreasing when the visible moisture level above the water plan starts stabilizing at around 25 cm ($t = 196$ h), which means that IRT is more efficient when the capillarity phenomenon is more intense.

The level of rising damp measured by the moisture detector follows the trend of the visible level and of the temperature difference until $t = 268$ h. After that instant, it continues increasing until the hygric equilibrium is achieved. The higher level of the rising damp measured with the moisture detector was expected as IRT only detects surface evaporation and the moisture detector assesses inner moist. Further analysis concerning this specific issue can be found in Barreira et al. (2016). These results are in line with the ones obtained by Camino et al. (2014), although in their work moisture has been assessed through a destructive methodology.

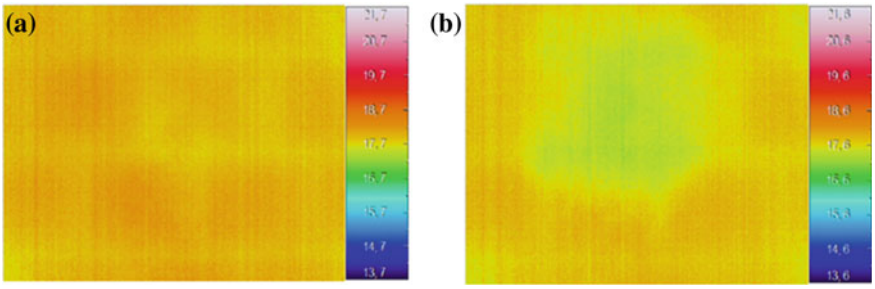

Fig. 3.16 Thermal image taken to assess surface condensation: **a** before spraying the surface; **b** immediately after spraying the surface

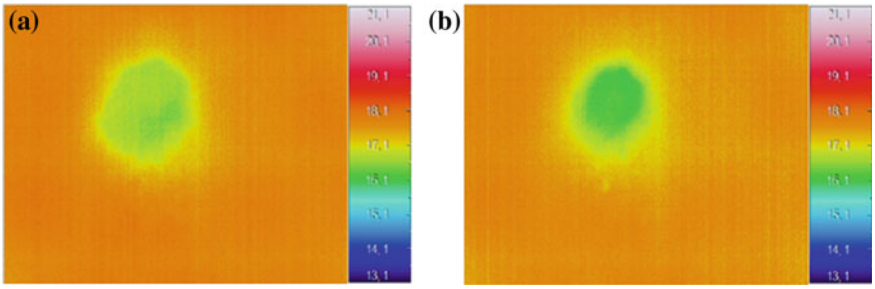

Fig. 3.17 Thermal image taken to assess surface condensation: **a** 15 min after spraying the surface; **b** 30 min after spraying the surface

3.3.2 Drying Process

To assess the drying process, a typical brick wall covered with painted rendering was used. Figures 3.16, 3.17, 3.18, 3.19 and 3.20 show the thermal images taken before and immediately after the spraying and during the drying period. Figure 3.16a shows that the wall was dry before it was sprayed with water. This conclusion is also supported by the results of the moisture detector (Fig. 3.21a).

After spraying the surface, the moist area was immediately detected on the thermal images through a limited colder area, which indicates a more intense evaporation. This area decreased during the drying process, especially in the first hour. Also, the temperature difference between the wet and dry areas decreases over time. After the first hour, the stained area was hardly visually detected and could only be detected through IRT. At the end of the test, no stained area could be detected in the thermal image (Fig. 3.20b).

The results of the moisture detector during the drying process were not reliable as no moisture was detected. In fact, the results obtained before spraying the surface and immediately after (Fig. 3.21) are very similar and do not indicate the presence

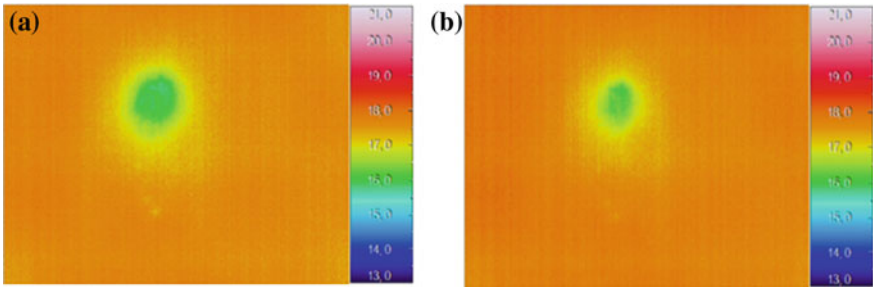

Fig. 3.18 Thermal image taken to assess surface condensation: **a** 45 min after spraying the surface; **b** 1 h after spraying the surface

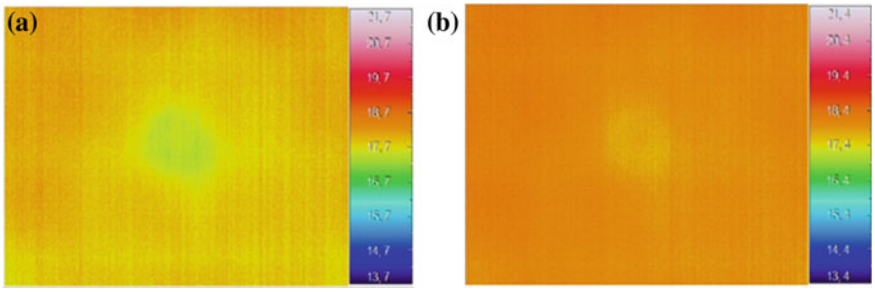

Fig. 3.19 Thermal image taken to assess surface condensation: **a** 4 h after spraying the surface; **b** 28 h after spraying the surface

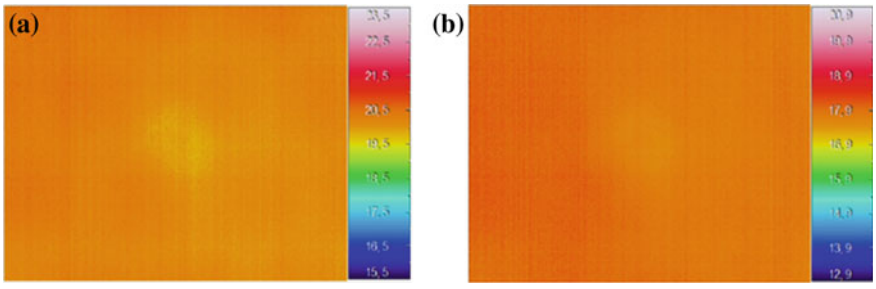

Fig. 3.20 Thermal image taken to assess surface condensation: **a** 124 h after spraying the surface; **b** 244 h after spraying the surface

of any moisture. Yet, this result was already expected, since the moisture detector only assesses inner moist.

Figures 3.22 and 3.23 show the time variation of the relative moist area (ratio between moist and dry area) and the difference between the maximum temperature (on the dry area) and minimum temperature (on the moist area).

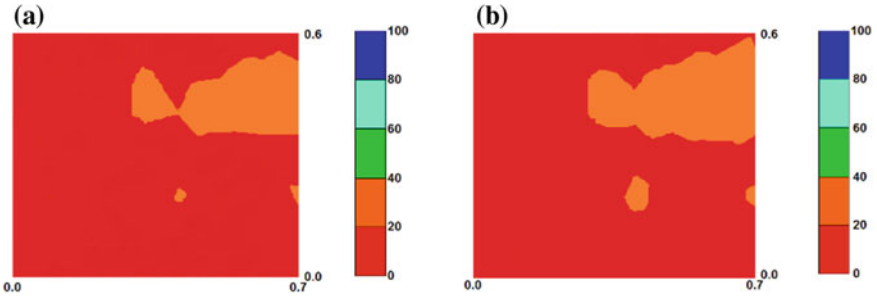

Fig. 3.21 Results of the moisture detector when assessing surface condensation: **a** before spraying the surface; **b** immediately after spraying the surface

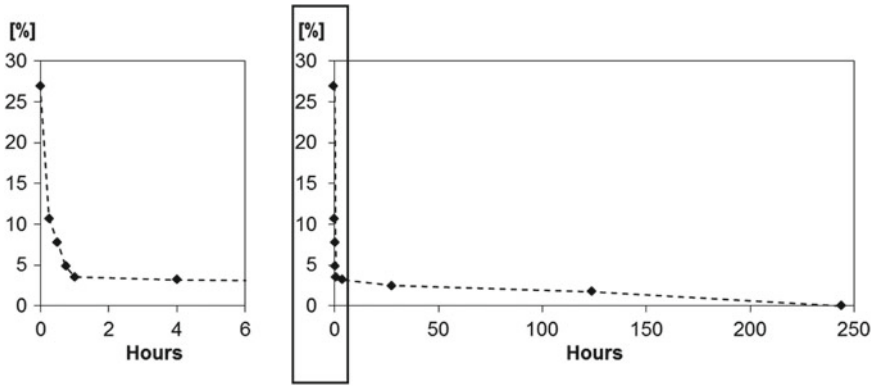

Fig. 3.22 Time variation of the relative moist area (ratio of moist and dry area)

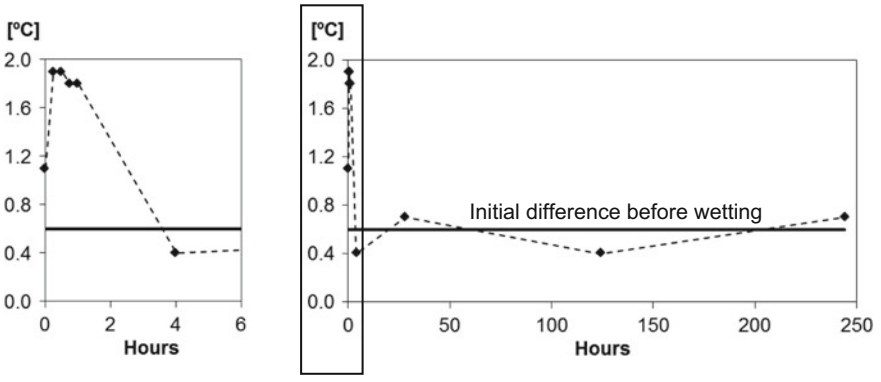

Fig. 3.23 Time variation of the difference between the maximum temperature (on the dry area) and minimum temperature (on the moist area)

The results point in the same direction of the qualitative analysis. Indeed, the stained area due to moisture decreased throughout the period of analysis, and the higher variations occurred in the first hour. After that period, the relative moist area was lower than 3.5%, indicating a stabilization of the drying process as no relevant deviations can be found (Fig. 3.22).

The temperature difference between the dry and wet areas (Fig. 3.23) was used to assess the drying process. The results confirm that the first hour was the most import. In fact, temperature differences were around 2 °C in the first hour, dropping to around 0.6 °C, which was the difference measured before the wetting process. It must be stated that there was an increase in the temperature difference in the first 15 min of drying that may be related to the intensity of water evaporation at the surface, which was lower immediately after spraying the surface.

3.4 Discussion of the Results

A new approach based on a common colour scale was applied both in IRT and in moisture readings and was tested on full-scale experimental set-ups. With this procedure, the IRT potential to assess moist areas due to capillarity and during the drying process was highlighted. Specific situations that cannot be visually detected were identified by IRT as the transition between the wet and dry surfaces of the specimens.

When assessing rising damp, generally, there is a good agreement between the thermal images and the readings of the moisture detector. However, the moisture detector points to a higher level of moisture, because IRT only detects surface evaporation, while the moisture detector assesses inner moisture. This is in accordance with numerical simulation performed by other authors, whose results confirm that the moisture level at the surface is lower than at mid-thickness of the specimen.

When evaluating the drying process, it was not possible to achieve an agreement between IRT and the moisture detector, because only superficial moisture was assessed and, therefore, the moisture detector was not able to detect it. However, IRT allowed understanding the critical period for the drying, not only in terms of stained area but also when assessing temperature differences between the stained and dried areas.

References

Avdelidis N, Moropoulou A, Theoulakis P (2003) Detection of water deposits and movement in porous materials by infrared imaging. Infrared Phys Technol 44(3):183–190

Balaras C, Argiriou A (2002) Infrared thermography for building diagnostics. Energy Build 34(2):171–183

Barreira E, Almeida RMSF, Delgado JMPQ (2016) Infrared thermography for assessing moisture related phenomena in building components. Constr Build Mater 110:251-69

Camino MS, León FJ, Llorente A, Olivar JM (2014) Evaluation of the behavior of brick tile masonry and mortar due to capillary rise of moisture. Mater Constr 64(314)

Edis E, Flores-Colen I, Brito J (2014) Passive thermographic detection of moisture problems in façades with adhered ceramic cladding. Constr Build Mater 51:187–197

Guimarães AS, Delgado JMPQ, Freitas VP (2010) Mathematical analysis of the evaporative process of a new technological treatment of rising damp in historic buildings. Build Environ 45(11):2414–2420

Menezes A, Gomes MG, Flores-Colen I (2015) In-situ assessment of physical performance and degradation analysis of rendering walls. Constr Build Mater 75:283–292

Chapter 4
IRT Versus Moisture: In Situ Tests in Indoor Environment

4.1 Aim

The favourable results obtained when using IRT to assess moisture in full-scale models, under controlled conditions in the laboratory, promoted a new test campaign in order to evaluate the applicability of this technique to detect moisture now in walls of buildings in use. Also, the promising results of other authors when using IRT to assess moisture in situ (Avdelidis et al. 2003; Grinzato et al. 2010; Lerma et al. 2011; Edis et al. 2014, 2015; Menezes et al. 2015) encouraged this new stage. During this campaign, the passive approach was implemented and moisture was detected due to the effect of evaporative cooling.

Moisture in the walls under study had two different sources: rising damp and infiltration of rainwater. Rising damp was assessed in an exterior wall of a basement in a residential building, and infiltration of rainwater were evaluated in three locations, two exterior walls of a room in a residential building and in a wall of a classroom. The thermal images were compared with the results provided by a moisture detector.

4.2 Materials and Techniques

The devices used in this campaign were an infrared camera (Fig. 3.4a) and a moisture detector (Fig. 3.4b). The main specifications of the equipment are described in Sect. 3.2.2. Three different case studies were analysed, each with different sources (rising damp and infiltrations) causing the moisture problems:

- Exterior wall of a basement in a residential building (Fig. 4.1a), where the moisture source was rising damp;
- Exterior wall of a classroom in (Fig. 4.1b);
- Exterior walls of a room in a residential building (wall 1 in Fig. 4.1c and wall 2 in Fig. 4.1d), where infiltrations from rainwater occurred.

E. Barreira and R. M. S. F Almeida, *Infrared Thermography for Building Moisture Inspection*, SpringerBriefs in Applied Sciences and Technology,
https://doi.org/10.1007/978-3-319-75386-7_4

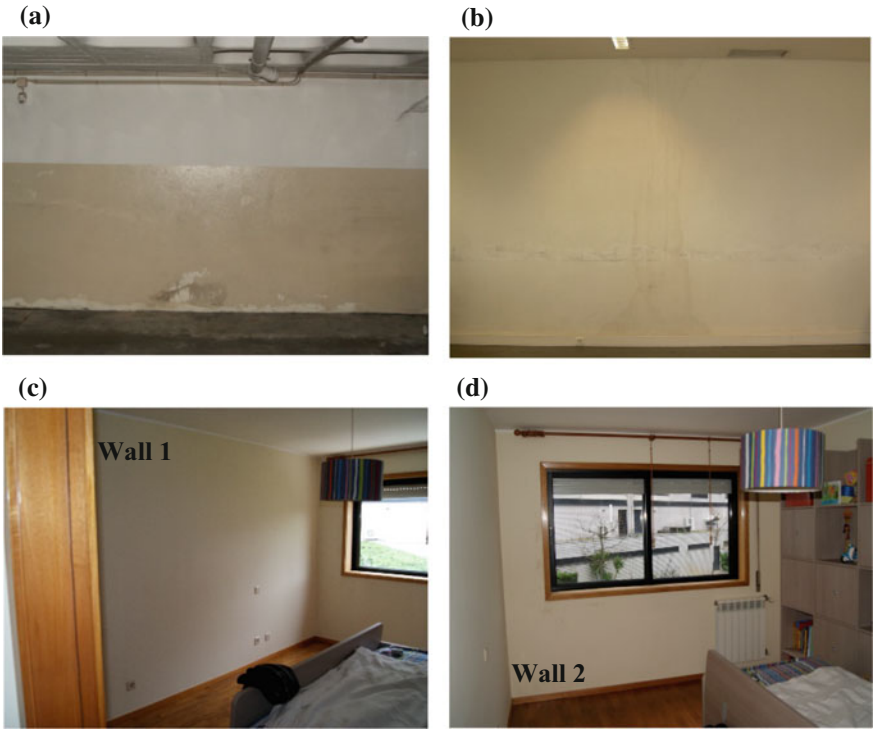

Fig. 4.1 Elements under study: **a** exterior wall of a basement in a residential building; **b** wall 1 of a room in a residential building; **c** wall 2 of a room in a residential building; **d** wall of a classroom in University of Porto

In this work, the IRT passive approach was used and the moist areas in the building components were assessed considering the effect of evaporative cooling. Thermal images were taken assuming an emissivity of 0.9 in the three set-ups because all walls were covered with cement plaster painted with light colour. The measurements were carried out after a rainy week.

To compare the results obtained by IRT with the ones provided by the moisture detector, the correlation between the relative scale of the detector results and the thermal images presented in Sect. 3.2.1 was used. Table 4.1 presents the characteristics of the grid used in each set-up. The spacing between dots depended on the area with visible degradation and the total area of the element (Barreira et al. 2016).

Table 4.1 Spacing between dots in the grids (in meters) for the assessment with the moisture detector

	Classroom	Room		Basement
		Wall 1	Wall 2	
Horizontal	0.30	0.30	0.30	0.20
Vertical				
Sound area	0.30	0.30	0.30	0.40
Damaged area	0.30	0.30	0.30	0.30

4.3 Results

4.3.1 Exterior Wall of a Basement in a Residential Building

The wall under study showed signs of degradation of the inner coating near the ground caused by rising damp (Fig. 4.1a). In the thermal image (Fig. 4.2a), a colder area near the ground, resulting from the evaporation of rising damp, is clearly displayed. The upper level of the colder area is above the visible degradation of the surface.

The results of the moisture detector (Fig. 4.2b) show that the moisture level in the wall was around 1.7 m from the ground, corresponding to a change in the superficial coating. The lower coating is less vapour permeable than the upper one, which can reduce superficial evaporation, increasing the amount of moisture in inner layers of the wall. When comparing the thermal image with the results of the moisture detector, they are not completely in accordance. One possible explanation may be related to the fact that IRT only detects surface evaporation, while the moisture detector assesses inner moisture.

The temperature profiles at 0.2 m from the ground (line A in Fig. 4.2a), at 0.7 m from the ground (line B in Fig. 4.2a) and at 1.2 m from the ground (line C in Fig. 4.2a), are displayed in Fig. 4.3. As expected, Line A, the nearest to the ground, presents the lower temperatures, followed by lines B and C. The temperature profile in line

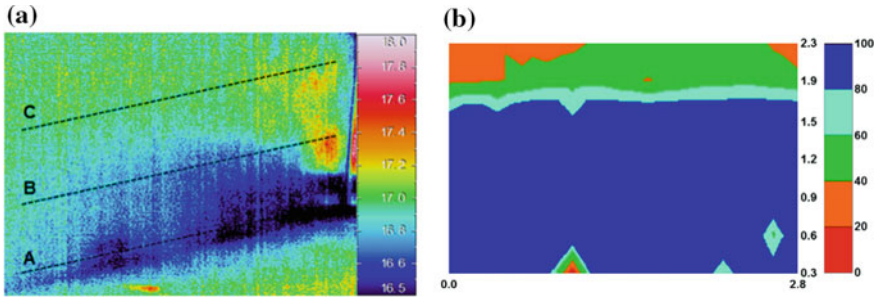

Fig. 4.2 Exterior wall of a basement in a residential building: **a** thermal image; **b** results of the moisture detector

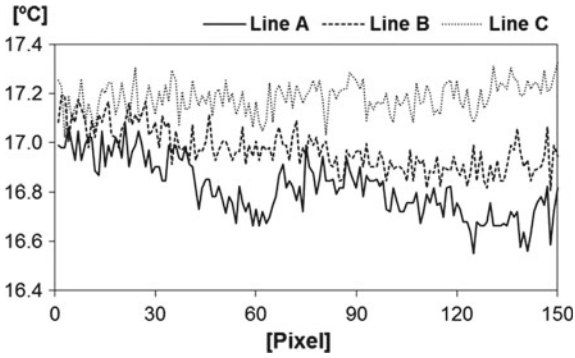

Fig. 4.3 Temperature profiles of an exterior wall of a basement in a residential building at 0.2 m from the ground through (line A), at 0.7 m from the ground (line B) and at 1.2 m from the ground (line C)

C indicates that the wall, at this level, was drier, because no relevant variations of the values between pixel 0 and 150 can be observed. In lines A and B, temperatures near pixel 150 are lower than the ones around pixel 0, which indicates higher moister problems near the corner.

Two critical zones can be pointed in line A, corresponding to the coating with greater degradation (between pixels 40 and 70 and between pixels 120 and 150, where temperatures are, on average, 16.8 and 16.7 °C, respectively). Due to the coating degradation, evaporation is more intense in these two zones and, thus, temperatures are lower.

The box plot representation of the temperature profiles at different levels (Fig. 4.4) points to higher variability of the values at line A and lower at line C. This result is due to a more intense evaporation at the bottom, where the highest amount of water is available, and also to the degradation of some areas of the coating that enhances the phenomenon. Smaller fluctuations in temperature at the highest level indicate that the amount of water reaching it is lower and temperature variations due to evaporation are not so evident.

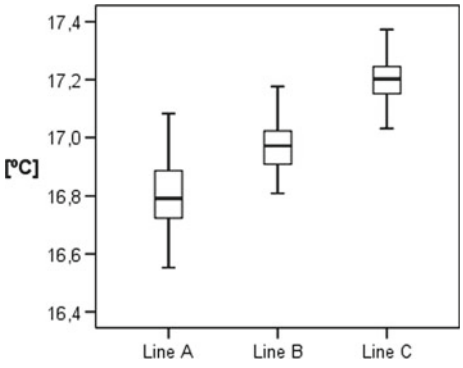

Fig. 4.4 Box plot representation of the temperature profiles of an exterior wall of a basement in a residential building at 0.2 m from the ground through (line A), at 0.7 m from the ground (line B) and at 1.2 m from the ground (line C)

4.3.2 *Exterior Walls of a Room in a Residential Building*

During the measurements, next to the corner and near the window, the coating of the two walls had visible signs of degradation caused by rainwater infiltration. The two walls were assessed individually (Fig. 4.1c, d). This infiltration had been detected before the test was performed and was not repaired by that time. Figure 4.5 shows the thermal images of the walls. The thermal images result from the assembly of individual images taken to restrict areas of each wall. Figure 4.6 shows the results obtained when using the moisture detector. Grey areas in Fig. 4.6a represent the position of the window and the radiator located in wall 1.

The thermal image of wall 1 displays lower surface temperatures around the left corner, under the window and at the top (Fig. 4.5a). The results of the moisture detector (Fig. 4.6a) showed that the wall is dry at the top, which indicates that the lower temperatures (dark blue) found in the thermal image correspond to a thermal bridge due to a beam. Although lower values have been measured with the moisture detector on the left vertical corner of the wall, at the thermal image, the lowest temperatures on this area (dark blue) are also related to a thermal bridge (structural column) and not only due to moisture. These considerations are supported by the information given by the structural plans of the building.

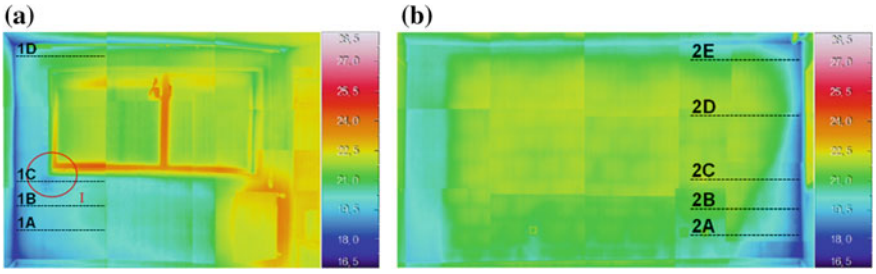

Fig. 4.5 Thermal images of the walls in a room: **a** wall 1; **b** wall 2

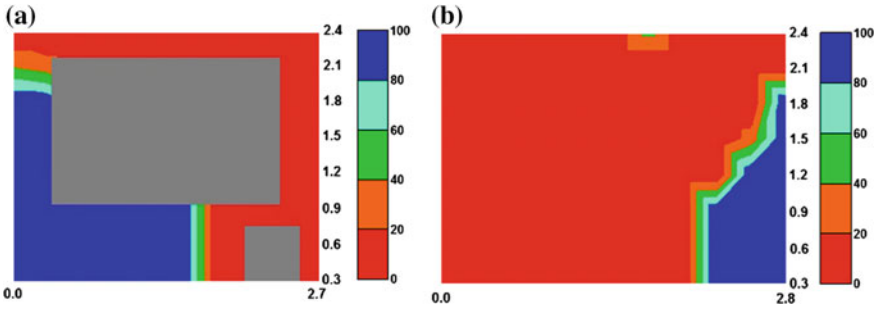

Fig. 4.6 Results of the moisture detector of the walls in a room: **a** wall 1; **b** wall 2

However, the surface temperature corresponding to the light blue colour results from the existence of moisture coming from outside. This conclusion was supported by the results of the moisture detector and by the existence of a damaged zone marked as I in Fig. 4.5a. Also, the visual inspection carried out on the exterior side of the wall revealed the existence of a crack. It must be stated that only the marked area is damaged in the inside. However, it is possible to assume that a larger area is affected by moisture, although not visually detected, taking into account the thermal image and the results of the moisture detector.

Figure 4.5b shows the thermal image of wall 2. Lower temperatures occur near the corners and at the top of the wall. The structural plans of the buildings indicate the presence of a beam and columns in those areas, which points to the existence of thermal bridges. However, there are clear differences between the colder areas on the left and right corners, indicating the presence of moisture in the right. The results of the moisture detector (Fig. 4.6b) support this conclusion, as the moister area is located near the right corner. Also, the existence of a crack on the exterior side of the wall in this area, as previously referred, strengthens this conclusion.

The temperature profiles of wall 1 at 0.3 m from the ground (line 1A in Fig. 4.5a), at 0.6 m from the ground (line 1B in Fig. 4.5a), at 0.9 m from the ground (line 1C in Fig. 4.5a) and at 2.4 m from the ground (line 1D in Fig. 4.5a) are displayed in Fig. 4.7. Figure 4.8 presents the temperature profiles for wall 2 (line 2A at 0.3 m, line 2B at 0.6 m, line 2C at 0.9 m, line 2D at 1.8 m and line 2E at 2.4 m in Fig. 4.5b).

Temperatures on lines 1A and 1B are very similar, although in line 1A the values are always lower. That may be related to the existence of a thermal bridge due to a beam. Although line 1C also presents temperatures similar to the ones of lines 1A and 1B, there are some critical areas between pixels 80 and 120 (point I in Fig. 4.5a) and between pixels 170 and 230, which are related to infiltrations of rainwater, as supported by the results of the moisture detector. Temperatures on line 1D are always higher as no moisture was detected at this level (Fig. 4.6a).

The temperature profiles of wall 2 (Fig. 4.8) show that at all levels there is an increase of surface temperature between pixels 0 and 10 related to a thermal bridge due to the existence of a column. However, at the lowest levels (lines 2A, 2B and

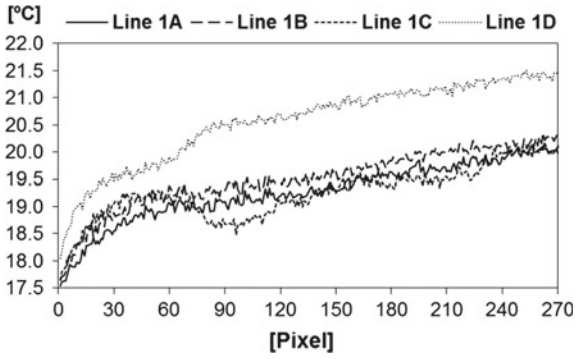

Fig. 4.7 Temperature profiles of wall 1 at 0.3 m from the ground through (line 1A), at 0.6 m from the ground (line 1B), at 0.9 m from the ground (line 1C) and at 2.4 m from the ground (line 1D)

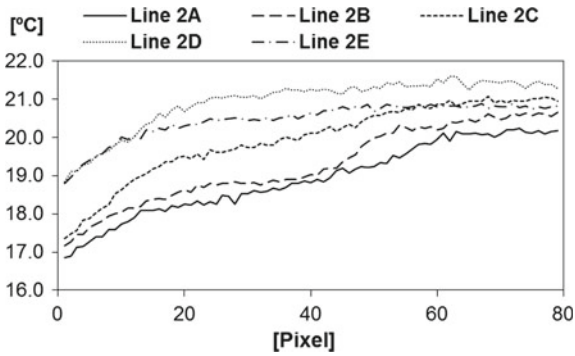

Fig. 4.8 Temperature profiles of wall 2 at 0.3 m from the ground through (line 2A), at 0.6 m from the ground (line 2B), at 0.9 m from the ground (line 2C), at 1.8 m from the ground (line 2D) and at 2.4 m from the ground (line 2E)

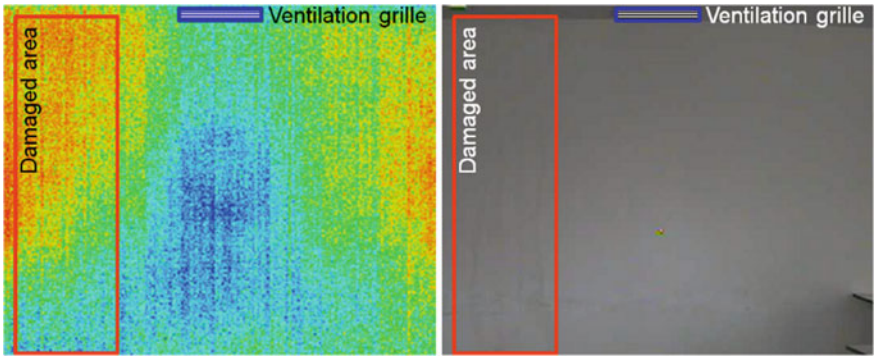

Fig. 4.9 Visible and thermal image of the wall under study in the classroom

2C), the superficial temperatures are lower, which indicates the existence of moisture that drops the values as a result of evaporation at the surface. Also, it is possible to detect that the moist area is larger at the bottom of the wall (line 2A) and decreases when the level is higher. In fact, the effect of moisture is noted until around pixel 60 at line 2A, around pixel 45 at line 2B and around pixel 20 at line 2C. Temperatures at lines 2D and 2E are very similar until around pixel 15, diverging from that point. The values are lower at line 2E due to the presence of a beam that decreases surface temperatures (thermal bridge).

4.3.3 Exterior Wall of a Classroom

By the time the measurements were carried out, the coating of the wall was damaged due to an infiltration of rainwater through the roof. This problem had already been detected and repaired two months before the test was performed. Figure 4.9 shows, respectively, the visible and the thermal image, and Fig. 4.10 shows the results of the moisture detector.

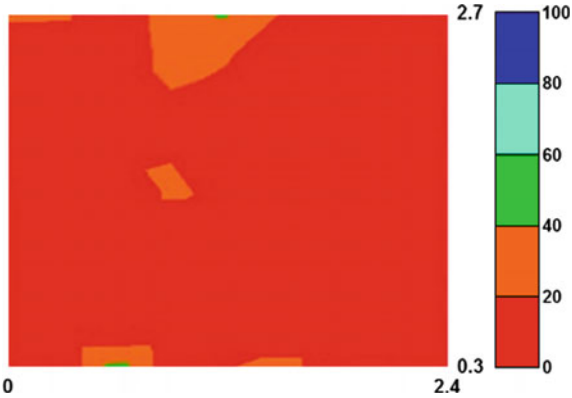

Fig. 4.10 Moisture detector results of the wall in the classroom

If not analysed carefully, the thermal image could lead to a misinterpretation of the results. In fact, the colder area (dark blue in Fig. 4.9) is not located where the coating is damaged but aligned with the ventilation grille located in the ceiling. The results of the moisture detector confirmed that there is no moisture in the wall, what was expected as the problem had already been repaired.

4.4 Discussion of the Results

Experimental tests showed that IRT is a valid diagnostic tool to evaluate moisture in building elements, when the source of humidity is rising damp and infiltrations of rainwater. However, in order to achieve reliable results, in some situations, it must be combined with other devices, namely a moisture detector to avoid misinterpretations.

Although moisture can be detected using the qualitative approach, the quantitative one proved to be very efficient, allowing extracting additional information. In fact, using the quantitative analyses of the thermal images, it was possible to identify critical areas that were not detected visually. These areas were highlighted by not only a sharp drop of surface temperature but also a larger variability of the values.

The use of complementary devices and/or information to support the findings of IRT proved to be of relevance. In two of the three case studies presented, misinterpretation of the results could have been a problem if a moisture detector was not used and if the structural plans of the building had not been analysed.

References

Avdelidis N, Moropoulou A, Theoulakis P (2003) Detection of water deposits and movement in porous materials by infrared imaging. Infrared Phys Technol 44(3):183–190

Barreira E, Almeida RMSF, Delgado JMPQ (2016) Infrared thermography for assessing moisture related phenomena in building components. Constr Build Mater 110:251–269

Edis E, Flores-Colen I, Brito J (2014) Passive thermographic detection of moisture problems in façades with adhered ceramic cladding. Constr Build Mater 51:187–197

Edis E, Flores-Colen I, Brito J (2015) Quasi-quantitative infrared thermographic detection of moisture variation in facades with adhered ceramic cladding using principal component analysis. Build Environ 94:97–108

Grinzato E, Cadelano G, Bison P (2010) Moisture map by IR thermography. J Mod Opt 57(18):1770–1778

Lerma JL, Cabrelles M, Portalés C (2011) Multitemporal thermal analysis to detect moisture on a building façade. Constr Build Mater 25(5):2190–2197

Menezes A, Gomes MG, Flores-Colen I (2015) In-situ assessment of physical performance and degradation analysis of rendering walls. Constr Build Mater 75:283–292

Chapter 5
IRT Versus Drying: In Situ Tests in Outdoor Environment

5.1 Aim

In this work, the applicability of IRT to assess the drying process of exterior walls after a long-term rainy period was evaluated through in situ tests. The physical phenomenon underlying these measurements was the effect of evaporative cooling and the passive approach was implemented. Simultaneously, a moisture detector was also used to qualitatively assess the evolution of the moisture content of the walls.

The walls under study were coated with similar rendering and painting, but they presented different orientations and, consequently, different exposure to solar. Differences in the exposure to thermal radiation were also found due to nearby obstacles that might have affected the drying process. However, they all presented clear visible signs of the presence of moisture (Barreira et al. 2016).

5.2 Materials and Techniques

The devices used in this campaign were an infrared camera (Fig. 3.4a) and a moisture detector (Fig. 3.4b). The main specifications of the equipment are described in § 3.2.2. The test campaign started when the rain period stopped and the measurements were carried out during six consecutive days, at 10:00, 12:00, 14:00, 16:00 and 18:00 (without solar radiation). Four walls with one-coat mortar as rendering were assessed. Figure 5.1 shows the orientation of the walls and the reference number of each case study. Moisture readings on the walls were made at three different points on each wall (Fig. 5.2).The position of the camera and the points on the walls were always the same.

For the IRT measurements, emissivity was set to 0.9. This value may not correspond to the real emissivity value of the surfaces under study; however, as only the qualitative approach was used, an estimated value of emissivity was considered

E. Barreira and R. M. S. F Almeida, *Infrared Thermography for Building Moisture Inspection*, SpringerBriefs in Applied Sciences and Technology,
https://doi.org/10.1007/978-3-319-75386-7_5

Fig. 5.1 Orientation of the walls and reference number of each case study

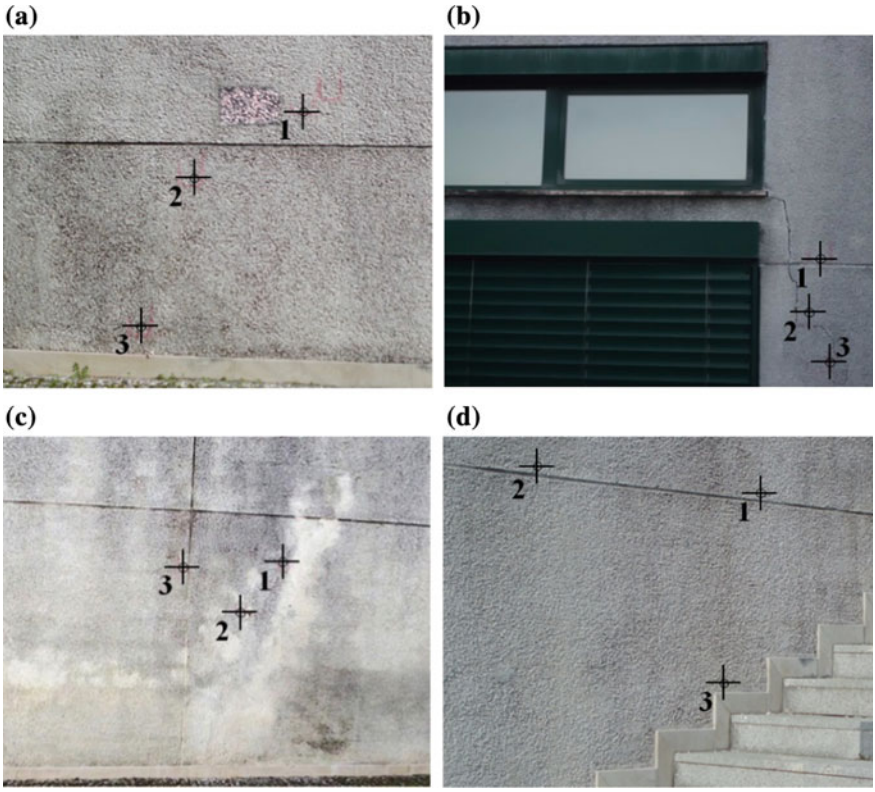

Fig. 5.2 Walls under study with measuring points: **a** Wall 1; **b** Wall 2; **c** Wall 3; **d** Wall 4

acceptable. Correction parameters were introduced before the IRT measurements began. Weather data (temperature, relative humidity, solar radiation and wind velocity and direction) was measured by a weather station located near the walls (Table 5.1).

Table 5.1 Average air temperature, relative humidity, solar radiation and wind velocity and direction measured by the weather station and qualitative evaluation of the climate

Day	Hour	T_{air} (°C)	RH_{air} (%)	Solar Rad (W/m^2)	Wind Vel/Dir (m/s)/(°)	Qualitative evaluation of the climate
1	10:00	9.8	64.1	553	12.2/301.5	Clear sky
	12:00	12.2	57.8	769		
	14:00	14.1	51.0	727		
	16:00	15.2	49.8	422		
	18:00	13.3	66.2	23		
2	10:00	11.0	72.6	559	10.1/117.0	Clear sky, after a foggy night
	12:00	16.0	48.2	766		
	14:00	17.9	40.8	731		
	16:00	18.3	39.7	429		
	18:00	17.1	44.2	22		
3	10:00	14.5	52.3	568	12.2/175.5	Clear sky
	12:00	17.5	32.2	783		
	14:00	19.4	29.3	734		
	16:00	19.8	31.0	422		
	18:00	18.3	41.1	20		
4	10:00	16.0	45.4	567	16.6/94.5	Clear sky
	12:00	19.0	38.6	780		
	14:00	20.6	27.4	742		
	16:00	20.2	29.8	425		
	18:00	17.5	30.2	24		
5	10:00	14.9	34.7	374	10.8/112.5	Cloudy sky
	12:00	18.3	30.2	387		
	14:00	21.0	25.7	516		
	16:00	19.4	31.2	165		
	18:00	16.8	33.1	22		
6	10:00	12.9	46.7	628	25.2/85.5	Clear sky
	12:00	16.0	39.9	842		

(continued)

Table 5.1 (continued)

Day	Hour	T_{air} (°C)	RH_{air} (%)	Solar Rad (W/m^2)	Wind Vel/Dir (m/s)/(°)	Qualitative evaluation of the climate
	14:00	17.4	38.5	783		
	16:00	17.3	44.9	470		
	18:00	14.1	76.4	36		

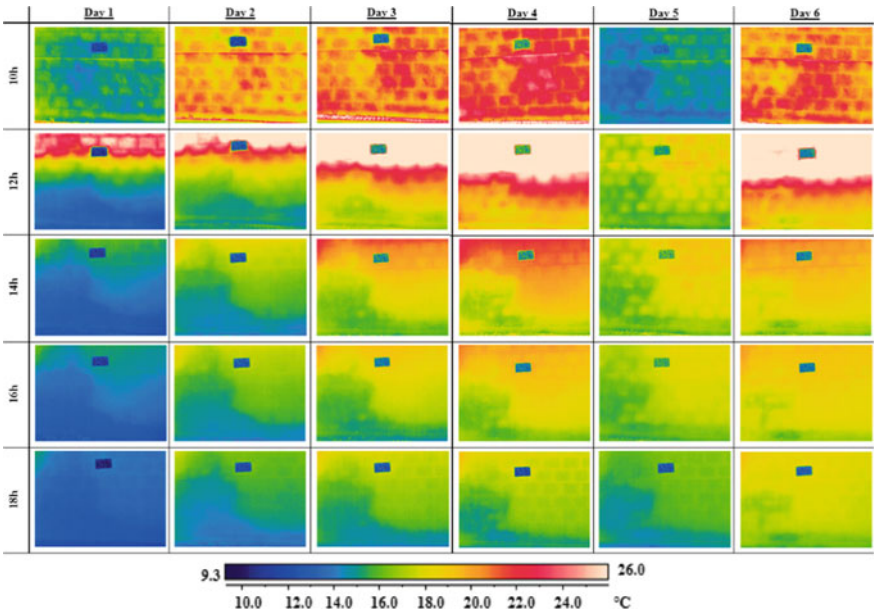

Fig. 5.3 Thermal images—wall 1

5.3 Results

5.3.1 Wall 1

The thermal images taken in wall 1 are shown in Fig. 5.3. The thermal images show that temperatures vary with the hour of the day. They also show that in the first day, the superficial temperatures on the wall were lower than the ones obtained at the end of the test campaign.

Temperatures were higher at 10:00 and at 12:00 because there was direct solar radiation on the wall. During these periods is difficult trying to assess moisture because the effect of sun as a heat source enhances other phenomena rather than moisture, as detachments and materials with different thermal properties (Freitas

et al. 2014). Considering the thermal images taken in the afternoon, the temperature values were always lower at 18.00, what was expected as air temperatures are also lower (Table 5.1).

Over the six days of measurements and considering only the thermal images taken at 16:00 and 18.00, there is a clear increase of the surface temperature and a decrease of the area with the lowest temperatures. Although the air temperature generally increased over time, it is possible to say that the wall was drying out because, for similar air temperatures, the temperature values on the wall increased. Taken as an example days 2 and 6 at 18:00, the temperature of the air was 17.1 and 14.1 °C, respectively, and temperatures on the wall were higher in day 6. Darker colours on the thermal images on day 5 are related to the cloudy day that decreased the air temperature and, consequently, the surface temperature.

Based on the previous considerations, it is possible to point that the moist area was mainly located on the left side and at the bottom of the thermal image. Over time, it tended to decrease, and at the end of the measurement period, it was located mostly near the ground.

The results of the moisture detector (Fig. 5.4) support the findings of IRT. On the three points that were assessed, generally, moisture decreased not only over the day but also over the period of measurements. During day 1, there was an increase of moisture at the end of the day that may be related to the runoff of accumulated water on the wall surface. The increase of moisture at the beginning of each day, when compared with last reading of the previous day, was probably due to higher relative humidity of the air during the night that increased moisture at the surface.

Figure 5.4 also shows that point 1, at the highest level, dried out faster than the other two, and at day 6, the readings of the moisture detector were around zero. This may indicate that this part of the wall was less affected by rainwater. The decrease of moisture on point 3, at the lowest level, was sharper than on point 2, located at an

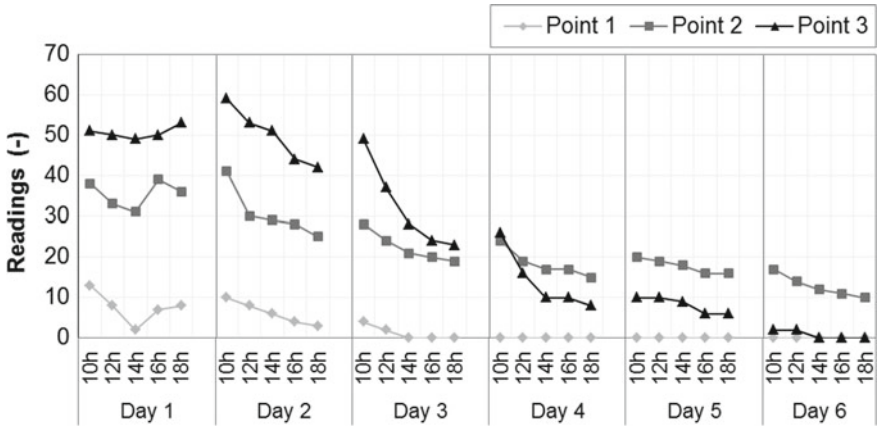

Fig. 5.4 Results of the moisture detector—wall 1

intermediate position. That can be explained because in the surroundings of point 2 there was a joint in the rendering, where accumulated water may have restricted the drying process.

5.3.2 Wall 2

The thermal images taken in wall 2 are shown in Fig. 5.5. The temperatures were higher during the afternoon because there was direct solar radiation on the wall. Shadows are clearly detected in the thermal images and may mask the effect of moisture at 14:00 and 16:00. However, some findings can be enhanced in the remaining results.

As in wall 1, also in this wall the increase of temperature on the right side is clear. There was an increase of the values not only over the day but also over the period of measurements. It is, however, difficult to detach the effect of air temperature, which increased the superficial temperature of the wall, from the increase of surface temperature due to the drop of moisture at the surface. However, when considering days with similar weather conditions, it is possible to notice that at the end of the measurement period the values were higher than at the beginning, pointing to less intense evaporation and, consequently, to a dryer surface.

The results of the moisture detector (Fig. 5.6) were in line with the ones of the thermal images, because moisture decreased over time at all levels. At the end of the

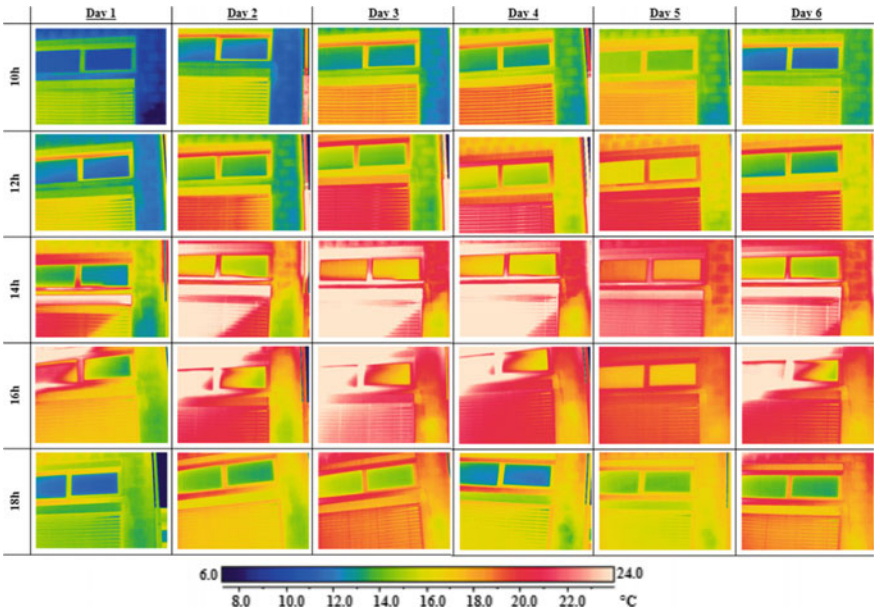

Fig. 5.5 Thermal images—wall 2

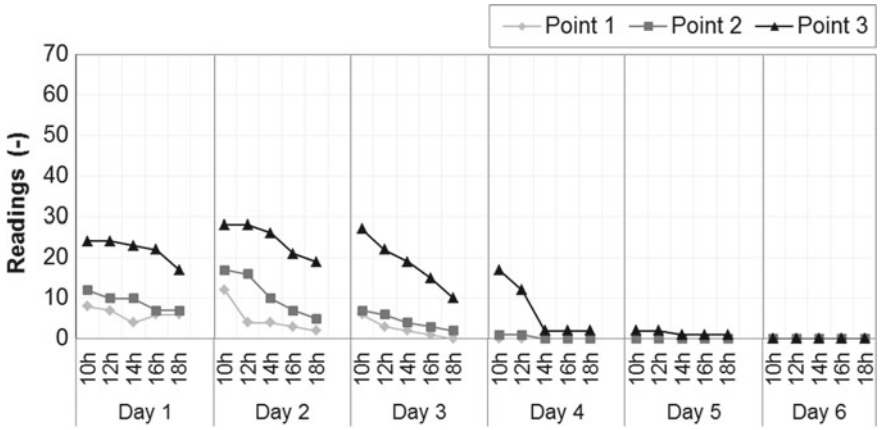

Fig. 5.6 Results of the moisture detector—wall 2

fourth day, the readings were very similar and around zero, indicating that the wall has dried out. Similar results on the three points were somehow expected since they were very close to each other.

5.3.3 Wall 3

The thermal images taken in wall 3 are shown in Fig. 5.7. Temperatures on this wall were lower than in the previous ones because there was no direct solar radiation. Although the effect of the sun was less relevant, these images are not completely conclusive regarding the drying process, mainly due to the thermal patterns resulting from dirt at the surface, different thermal conductivity of the inner layers and/or influence of the surrounding environment, which are problems also verified by Rumbayan and Washer (2014).

Although the results of IRT are not totally clear, the moisture content indicates that the wall dried out over time as at the end of day 6 the readings at all levels were around zero (Fig. 5.8).

5.3.4 Wall 4

As in wall 3, also in this case (Fig. 5.9) the results revealed that tackling the drying process in the outdoor exclusively through qualitative IRT is not straightforward, although a tendency for higher surface temperatures throughout the analysis can be identified. Yet, the air temperature was also increasing, which highlights the

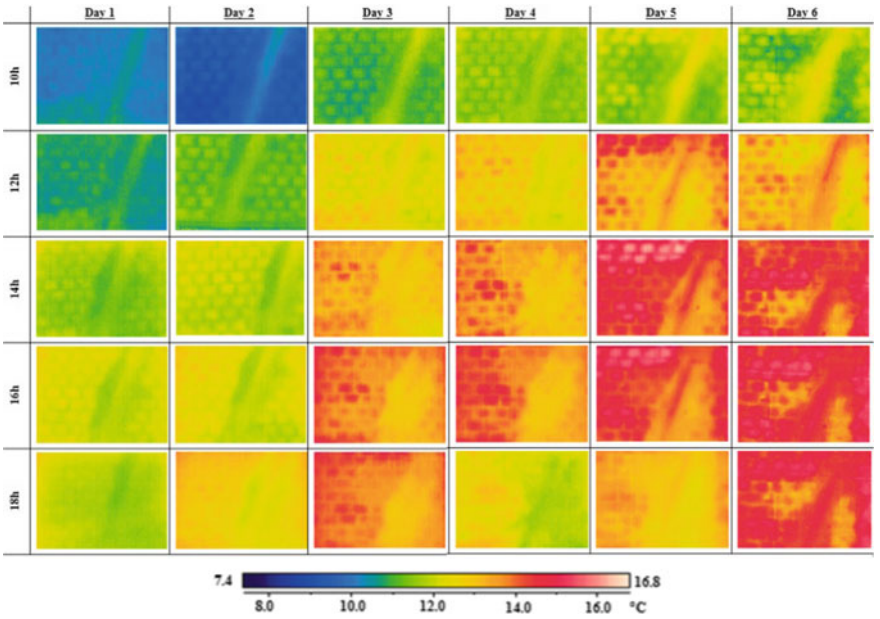

Fig. 5.7 Thermal images—wall 3

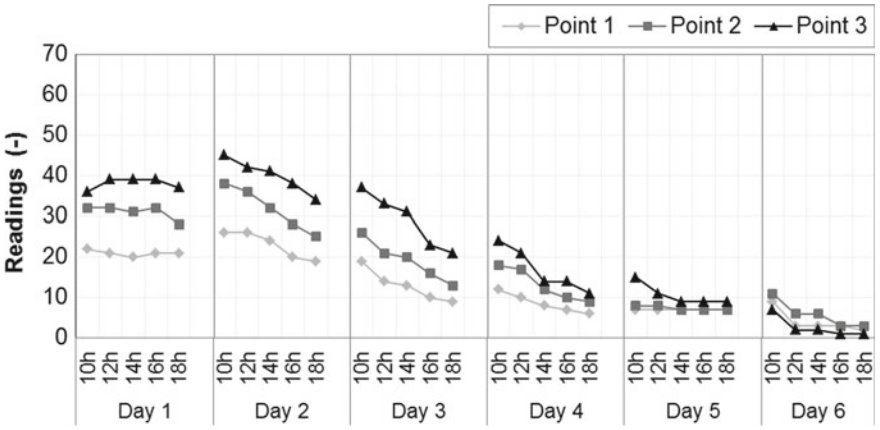

Fig. 5.8 Results of the moisture detector—wall 3

difficulty of isolating the effect of evaporative cooling. In addition, the influence of solar radiation in the thermal images is difficult to assess.

Lerma et al. (2014) could clearly visualise the relationship between evaporation and surface temperature of a material as at the beginning of the process the temperature falls and then tends to equalise the air temperature. However, this test was performed in laboratory, using small samples and under very controlled conditions.

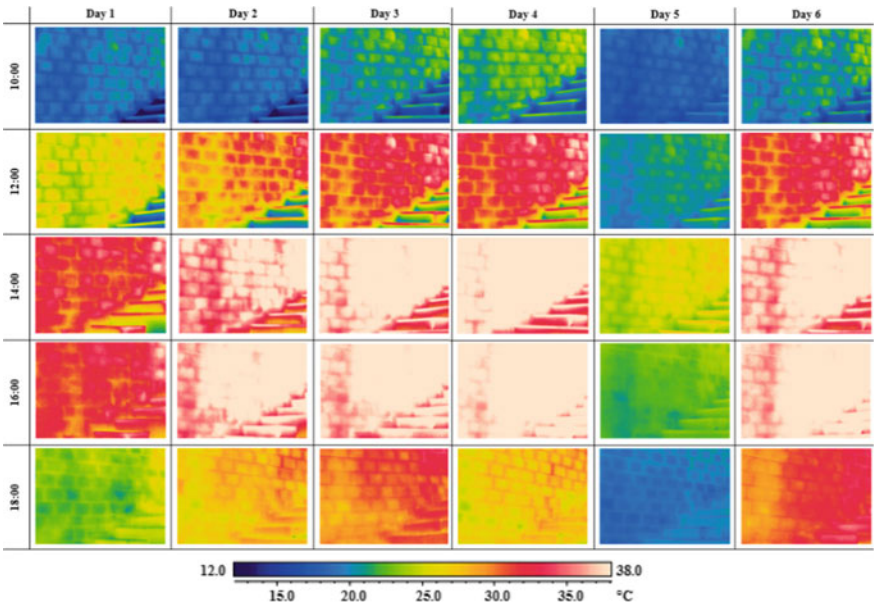

Fig. 5.9 Thermal images—wall 4

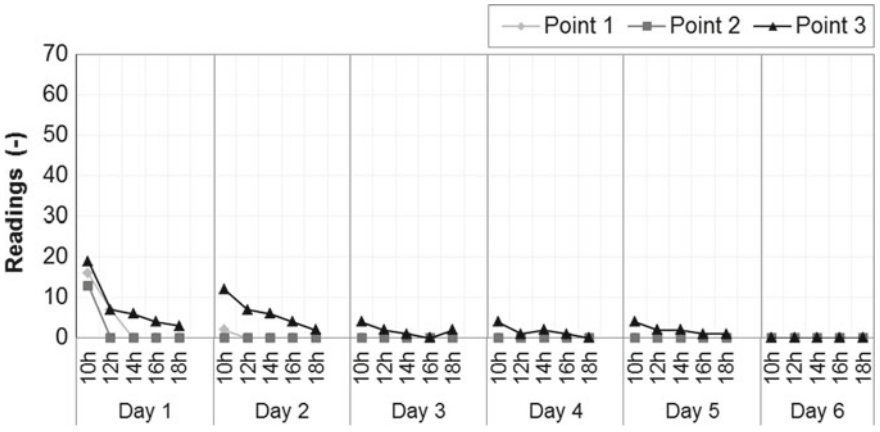

Fig. 5.10 Results of the moisture detector—wall 4

Figure 5.10 shows the results obtained with the moisture detector. From day 2, readings on point 1 and point 2 had null values, which mean that the wall was superficially dry. As expected, point 3 had higher moisture content as it was near the ground, where a larger amount of water was accumulated. However, at the end of day 6, it was also completely dry.

On the other hand, as expected, measurements on the wall 4, the only one facing south, presented lower values of moisture content because there was higher amount of incident solar radiation.

5.4 Discussion of the Results

The results of IRT to assess the drying process were not straightforward. The thermal images were strongly influenced by direct solar radiation, which highlighted other phenomena, like detachments, materials with different thermal characteristics and/or influence of the surrounding environment, sometimes masking the effect of surface evaporation. In addition, the air temperature significantly influenced the surface temperature of the wall, which could have led to misinterpretations of the results, if the time variation of the air temperature was not considered.

Although the restrictions previously indicated, it was possible to point out the drying process, when considering days with similar weather conditions. In fact, generally, at the end of the measurements the temperature values were higher than the ones at the beginning, pointing to less intense evaporation and, consequently, to a dryer surface.

The results of the moisture detector supported the findings of IRT. Generally, locations with higher values corresponded to areas with lower temperatures in the thermal images. Besides, the values of the readings decreased not only over the day but also over the period of measurements. The increase of moisture at the beginning of each day, when compared with last reading of the previous day, was probably due to higher relative humidity of the air during the night that increased moisture at the surface.

When comparing the four cases under study, it is possible to verify that wall 4 dried out faster than the other ones. At day 3, it was almost completely dry. The other walls needed at least 4 days (wall 2) or 6 days (walls 1 and 3) to achieve the same condition. That may be related to the fact that wall 4 was more exposed to direct solar radiation, which intensified surface evaporation.

References

Barreira E, Almeida RMSF, Delgado JMPQ (2016) Infrared thermography for assessing moisture related phenomena in building components. Constr Build Mater 110:251–269

Freitas SS, Freitas VP, Barreira E (2014) Detection of façade plaster detachments using infrared thermography—A non-destructive technique. Constr Build Mater 70:80–87

Lerma C, Mas Á, Gil E, Vercher J, Peñalver MJ (2014) Pathology of building materials in historic buildings. relationship between laboratory testing and infrared thermography. Materiales de Construcción 64(313):009

Rumbayan R, Washer GA (2014) modeling of environmental effects on thermal detection of subsurface damage in concrete. Res Nondestr Eval 25(4):235–252